

Accepted Manuscript

Structure and elasticity of phlogopite under compression: Geophysical implications

Tanvi D. Chheda, Mainak Mookherjee, David Mainprice, Antonio M. dos Santos, Jamie J. Molaison, Julien Chantel, Geeth Manthilake, William A. Bassett

PII: S0031-9201(14)00121-6

DOI: <http://dx.doi.org/10.1016/j.pepi.2014.05.004>

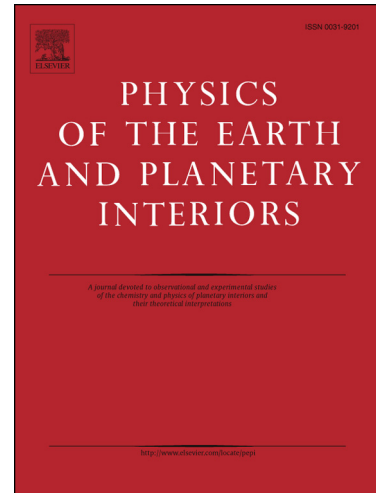
Reference: PEPI 5741

To appear in: *Physics of the Earth and Planetary Interiors*

Received Date: 3 December 2013

Revised Date: 24 March 2014

Accepted Date: 9 May 2014



Please cite this article as: Chheda, T.D., Mookherjee, M., Mainprice, D., dos Santos, A.M., Molaison, J.J., Chantel, J., Manthilake, G., Bassett, W.A., Structure and elasticity of phlogopite under compression: Geophysical implications, *Physics of the Earth and Planetary Interiors* (2014), doi: <http://dx.doi.org/10.1016/j.pepi.2014.05.004>

This is a PDF file of an unedited manuscript that has been accepted for publication. As a service to our customers we are providing this early version of the manuscript. The manuscript will undergo copyediting, typesetting, and review of the resulting proof before it is published in its final form. Please note that during the production process errors may be discovered which could affect the content, and all legal disclaimers that apply to the journal pertain.

24th March, 2014

Structure and elasticity of phlogopite under compression: Geophysical implications

Tanvi D. Chheda¹, Mainak Mookherjee^{1*}, David Mainprice², Antonio M. dos Santos³, Jamie J. Molaison³, Julien Chantel⁴, Geeth Manthilake⁴, and William A. Bassett¹

¹Earth and Atmospheric Sciences, Cornell University, Ithaca, NY 14850.

*Email: mainak.mookherjee@cornell.edu

²Geosciences Montpellier UMR CNRS 5243, Universite Montpellier 2, 34095 Montpellier cedex 05, France.

³Neutron Sciences Directorate, Oak Ridge National Laboratory, Oak Ridge, TN 37831.

⁴Laboratoire Magmas et Volcans, Universite Blaise Pascal, 63038 Clermont-Ferrand, France.

Abstract:

We investigated the response of the crystal structure, lattice parameters, and unit-cell volume of hydrous layered silicate phlogopite at conditions relevant to subduction zone settings. We have used *first principles* simulation based on density functional theory to calculate the equation of state and full elastic constant tensor. Based on the generalized gradient approximation, the full single crystal elastic constant tensor with monoclinic symmetry shows significant anisotropy with the compressional elastic constants: $c_{11} = 181$ GPa, $c_{22} = 185$ GPa, $c_{33} = 62$ GPa, the shear elastic constants- $c_{44} = 14$ GPa, $c_{55} = 20$ GPa, $c_{66} = 68$

Ga, and $c_{46} = -6$ GPa; the off diagonal elastic constants $c_{12} = 48$ GPa, $c_{13} = 12$ GPa, $c_{23} = 12$ GPa, $c_{15} = -16$ GPa, $c_{25} = -5$ GPa and $c_{35} = -1$ GPa at zero pressure. The elastic anisotropy of phlogopite is larger than most of the layered hydrous phases relevant in the subduction zone conditions. The shear anisotropy, AV_s for phlogopite is $\sim 77\%$ at zero pressure condition and although it decreases upon compression it remains relatively high compared to other hydrous phases relevant in the subduction zone settings. We also note that the shear elastic constants for phlogopite are relatively low. Phlogopite also has a high isotropic bulk V_p/V_s ratio ~ 2.0 . However, the V_p/V_s ratio also exhibits significant anisotropy with values as low as 1.49. Thus, phlogopite bearing metasomatized mantle could readily explain unusual V_p/V_s ratio as observed from seismological studies from the mantle wedge regions of the subduction zone.

Key words: Elasticity, Seismic Anisotropy, Hydrous phases, Subduction zone

1. Introduction

Phlogopite is a potassium bearing mica that is stable in hydrous ultrapotassic rocks. In particular, phlogopite occurs in hydrothermally altered oceanic crust and mantle. Phase stability studies show that phlogopite could be stable up to pressures of ~ 9 GPa (Yoder and Eugster, 1954; Yoder and Kushiro, 1954; Kushiro *et al.*, 1967; Trønnes, 2002) and has been thought to play an important role in generation of arc magmas (Sudo and Tatsumi, 1990). However, more recent studies have shown that, during the breakdown of phlogopite much of the water is partitioned into potassium amphibole, richterite, owing to the

similar K/OH ratio (Konzett and Ulmer, 1999). Only a small amount of aqueous fluid is released and this cannot account for the formation of the arc magmas (Konzett and Ulmer, 1999). The mantle wedge overlying subducting slabs is further hydrated by the release of such aqueous fluids. And at least a part of the incompatible elements such as potassium, partition into the released fluids that migrate upward and lead to widespread mantle metasomatism (Bailey, 1982). This stabilizes potassium bearing hydrated assemblages such as phlogopite bearing altered peridotite in the mantle wedge (Sekine and Wyllie 1982; Wyllie and Sekine, 1982) overlying the subducted slabs. Also, sub-cratonic lithosphere might be enriched in large ion lithophile elements (such as potassium) through metasomatism by hydrous silicate melts (Thompson, 1992). The bulk chemical compositions of altered rocks such as mica-amphibole-rutile-ilmenite-diopside (MARID) is very similar to the chemistry of phlogopite in a $(\text{Mg},\text{Fe})_2\text{SiO}_4$ (olivine)- SiO_2 (quartz)- $\text{K}_2\text{O}+\text{Na}_2\text{O}$ (alkali) ternary (Sweeney *et al.*, 1993). Hence, understanding the physical properties of phlogopite is likely to enhance our understanding of the thermodynamic stability of the altered rock assemblages. In addition, it is also important to constrain the elasticity of phlogopite and evaluate its role in explaining geophysical observations in the subduction zone settings. Most of the studies conducted so far have focused on the phase relations (e.g., Konzett and Ulmer, 1999; Sato *et al.*, 1996, 1997; Fumagalli *et al.*, 2009), crystal structure and equation of state of phlogopite (Rayner, 1974; Hazen and Finger, 1978; Pavese *et al.*, 2003; Comodi *et al.*, 2004; Gatta *et al.*, 2011). However, the full monoclinic elastic constant tensor of phlogopite has never been measured and till now, only the 5 independent constants of pseudo-

hexagonal symmetry have been reported in the literature (Alexandrov and Ryzhova, 1961; Alexandrov *et al.*, 1974).

In this study, we explore the crystal structure, equation of state, and full mononclinic elastic constant tensor of phlogopite at high-pressure using *first principles* simulation.

2. Method

2. 1. First principle simulations

We performed *first principles* quantum mechanical simulation based on density functional theory (DFT) (Hohenberg and Kohn, 1964; Kohn and Sham, 1965). Density functional theory has been widely used to study the structure, energetics and elasticity of mineral phases relevant to Earth and Planetary sciences (*e.g.* Oganov *et al.*, 2002). The DFT solution for the energies in the system considered is exact in principle, but the nature of the electronic many-body interaction is mapped onto a potential for exchange and correlation that needs to be approximated. We investigate phlogopite $[K(Mg)_3(Si_3Al)O_{10}(OH)_2]$ with two widely used approximations to the exchange-correlation functional: the generalized gradient approximation (GGA) (Perdew and Wang, 1986; Perdew *et al.*, 1991) and local density approximation (LDA) (Ceperley and Adler, 1980). In order to facilitate solving the DFT equations, further approximations were made, motivated by the argument that the core electrons participate little in bonding and structural changes. We have used widely accepted and highly accurate projector augmented wave method (PAW) (Kresse and Joubert, 1999) as implemented in the Vienna *ab initio* simulation package (VASP) (Kresse and Hafner, 1993; Kresse and Furthmüller, 1996a,b; Kresse and Joubert, 1999). We

determined the energy-volume relationship of the phlogopite phase using GGA and LDA with PAW methods. Phlogopite has a monoclinic, $C2/m$ space group symmetry (Redhammer and Roth, 2002). The aluminum and silicon atoms are ordered in the $T0_4$ tetrahedral sites. Although our calculations are static, we have ordered the aluminum and silicon atoms into the tetrahedral sites in distinct layers and to retain the monoclinic symmetry we doubled the c -axis. All computations were performed in the primitive unit-cell with a space group $P2_1/c$ with 88 atoms and Z=4 (**Figure 1**). We used an energy cut-off $E_{cut}= 500$ eV and a Monkhorst-Pack (Monkhorst and Pack, 1976) $2\times2\times2$ k -point mesh, yielding 2 k points in the irreducible wedge of the Brillouin zone. A series of convergence tests demonstrated that these computational parameters yield total energies that converge within 5 meV/atom. Previous studies have shown that density functional theory captures the relevant physics of hydrous minerals (Mookherjee and Stixrude, 2006; Mainprice *et al.*, 2008; Tsuchiya and Tsuchiya, 2009; Ortega-Castro *et al.*, 2010; Chantel *et al.*, 2012) with varying bond strengths from strong hydroxyls to the weak interlayer forces (Stackhouse *et al.*, 2004; Fumagalli and Stixrude, 2007; Mookherjee and Stixrude, 2009; Mookherjee and Capitani, 2011; Militzer *et al.*, 2011; Mookherjee and Bezacier, 2012; Hernandez-Haro *et al.*, 2013). Based on previous computational studies GGA often leads to more accurate predictions for the hydrogen bearing mineral systems (Tsuchiya *et al.*, 2005; 2008; Mookherjee and Stixrude, 2006). In addition to hydrogen bearing minerals, computational studies on molecular water (H_2O) and ice (Hamann, 1997) show that the GGA method (Perdew *et al.*, 1996) provided excellent predictions for energetics and elasticity of hydrogen bearing systems. However, LDA method has been successful in describing the

equation of state of layered hydrous phases such as talc (Stixrude, 2002; Stixrude and Peacor, 2002). Hence, we calculated the full elastic constant tensor of phlogopite using both the GGA and LDA method. To calculate the elasticity, we strained the lattice and allowed the internal degrees of freedom of the crystal structure to relax consistent with the symmetry: elastic constants were obtained through the changes in stress tensor (σ) with respect to applied strain (ϵ). For a specific volume, we applied positive and negative strains of magnitude 0.5%, 1%, and 2% and accurately determined the stresses. The elastic constants were then determined by the linear relation between the stress and strain in the appropriate limit of zero strain (Figure S1). We noted that 1% strain approximates the limit of zero strain as previously reported for most of the geologically relevant mineral phases (Karki *et al.*, 2001). Hence to remain in the field of linear elastic behavior we employed strains up to 1% to determine the elastic constants. An orthogonal reference frame used for computing the tensor may be X=a* Y=b/b* Z=c. We calculated the elastic anisotropy of phlogopite using petrophysical software (Mainprice, 1990).

3. Result

3. 1. Equation of state

The volume dependence of total energy obtained using DFT simulations with LDA and GGA approximations are adequately described by a third-order Birch-Murnaghan equation of state (Birch, 1978)

$$E = E_0 + \frac{9}{2} K_0 V_0 [(K'_0 - 4) f_v^3 + f_v^2] \quad (1)$$

where, E_0 , K_0 , V_0 , and K'_0 represents the ground state energy, bulk modulus at zero-pressure, unit-cell volume at zero-pressure, and pressure derivative of zero-pressure bulk modulus respectively.

and,

$$f_V = \frac{1}{2} \left(\left(\frac{V_0}{V} \right)^{\frac{2}{3}} - 1 \right) \quad (2)$$

The zero-pressure volume based on the LDA, V_0^{LDA} is 3 % smaller than the zero-pressure volume based on single crystal X-ray diffraction study, V_0^{\exp} (Hazen and Finger, 1978). All comparisons are made using conventional cell parameters (**Figure 2**). In contrast, zero-pressure volume based on the GGA, V_0^{GGA} is 6.4% larger than the experimental value (**Table 1**). The simulation results based on LDA and GGA tends to bracket the experimental V_0^{\exp} as $V_0^{LDA} < V_0^{\exp} < V_0^{GGA}$ and K_0^{\exp} as $K_0^{LDA} > K_0^{\exp} > K_0^{GGA}$ (**Figure 2, Table 1**). Experimental work on phengite mica, a *di*-octahedral mica also has a similar zero-pressure bulk modulus of ~ 57.0 (± 3.0) GPa (Smyth et al., 2000).

The linear bulk moduli were determined using linear finite strain expression (Davies 1974; Weaver, 1976; Meade and Jeanloz, 1990) and f_l - F_l relationships (**Figure 3, Table 2**)

$$F_l = K_l + m_l f_l \quad (3)$$

where F_l is the linear normalized pressure, given by

$$F_l = \frac{P}{f_l(1+2f_l)(1+2f_V)} \quad (4)$$

and f_l is the linear Eulerian finite strain, given by

$$f_l = \frac{1}{2} \left(\left(\frac{l_0}{l} \right)^2 - 1 \right) \quad (5)$$

and f_V is the volume Eulerian finite strain, as defined above in eq. (2). The linear bulk moduli along a -, b -, and c -axis directions follow the relation $K_b^{GGA} > K_a^{GGA} > K_c^{GGA}$. Similar relations are also observed for the LDA results and previous experimental studies (Pavese *et al.*, 2003). The simulation results based on LDA and GGA tends to bracket the experimental linear bulk moduli K_l^{exp} (Pavese *et al.*, 2003) as $K_l^{\text{LDA}} > K_l^{\text{exp}} > K_l^{\text{GGA}}$ where $l = a$ -, b -, and c^* -axis respectively (**Figure 3**, **Table 2**), where $c^* = c \sin\beta$. The bulk modulus calculated from the linear moduli $K_0 = [K_a^{-1} + K_b^{-1} + K_{c^*}^{-1}]$ are consistent for GGA, LDA, and the experimental study (Pavese *et al.*, 2003) within 1.9 %, 2.7 %, and 1.4 % respectively. However, the bulk modulus calculated using the linear moduli reported for the single crystal X-ray diffraction study (Comodi *et al.*, 2004) is not consistent with more than 67 % difference. The likely cause for this difference is related to the incorrect use of a third order finite strain equation for linear-moduli, rather than using the finite strain formulations, i.e., eq (3) to (5).

3. 2. Structure

Phlogopite is a layered hydrous silicate with tetrahedral units linked to form *di*-trigonal rings. An octahedral layer is sandwiched by two such tetrahedral sheets with the tetrahedral apex pointing towards each other (**Figure 1**). The region between two successive tetrahedral-octahedral-tetrahedral (T-O-T) sheets is called the interlayer region, which hosts the large potassium atom. Upon compression, the tetrahedral units remain stiff, with a

zero-pressure bulk modulus $K_{TO_4,0}^{GGA} = 241.0$ GPa, where TO_4 refers to the tetrahedral unit ($T=Si, Al$). The octahedral units are more compressible with a zero pressure bulk modulus $K_{MO_6,0}^{GGA} = 112.1$ GPa, where MO_6 refers to the octahedral unit ($M=Mg, Al$). The interlayer region is characterized by relatively large compression with a zero pressure bulk modulus $K_{KO_{12},0}^{GGA} = 21.1$ GPa, (**Figure 4, Table 3**). Upon heating, the interlayer region also undergoes significantly larger expansion compared to the other structural units (Mookherjee and Redfern, 2002). The main compression along the a - b plane is accommodated by in-plane rotation of tetrahedral units, characterized by the angle, α . For a perfect hexagonal ring, $\alpha = 0^\circ$, as the hexagonal ring deforms to *di*-trigonal ring where $\alpha > 0^\circ$. Upon compression, the degree *di*-trigonal distortion increases as shown by the increase of the angle as a function of pressure. Similar behaviour is also observed in previous single crystal x-ray diffraction study (Comodi *et al.*, 2004) (**Figure 4**). The behaviour of α upon compression is opposite when layered silicates expand on heating, *i.e.* α tends to decrease when a layered hydrous silicate undergo thermal expansion leading to decrease of the *di*-trigonal distortion (Mookherjee *et al.*, 2001; Chon *et al.*, 2006). Upon compression, the hydroxyl (OH) bond length (r_{OH}) remains largely unchanged and the corresponding O---H and O---O distances, *i.e.*, r_{O-H} and r_{O-O} decrease (**Figure 4**). Within the pressure range of our study we do not find any evidence of hydrogen bonding since the O-H bond lengths do not increase upon compression, as documented in hydrogen-bonded systems.

3. 3. Elasticity

Phlogopite has monoclinic symmetry with 13 independent elastic constants, three compressional elastic constants- c_{11}, c_{22}, c_{33} , three shear elastic constants- c_{44}, c_{55}, c_{66} and seven off diagonal elastic constants- $c_{12}, c_{13}, c_{23}, c_{15}, c_{25}, c_{35}$, and c_{46} (Nye 1985). As a result of low symmetry and the rarity of obtaining gem quality single crystals, very few experimental data on the elasticity of phlogopite exist (Alexandrov and Ryzhova, 1961; Alexandrov *et al.*, 1974). The calculated elastic constants are in excellent agreement with the experimental data (**Figure 5**). Among the principal elastic components- $c_{11} \sim c_{22} > c_{33}$, whereas the off-diagonal elastic constant show the relation- $c_{12} > c_{13} \sim c_{23}$ and $c_{35} > c_{25} > c_{15}$. The shear elastic constants follow the relation- $c_{66} > c_{55} > c_{44} > c_{46}$ (**Figure 5**). The relationship holds for both LDA and GGA methods and all pressures. Pressure dependence of elasticity data could be described by finite strain formulation (in full 4th rank tensor notation)

$$c_{ijkl} = (1 + 2f_V)^{3.5} \left[c'_{ijkl0} + b_1 f_V + 0.5 b_2 f_V^2 \right] - P \Delta_{ijkl}, \quad (8)$$

where, f_V is the finite strain as defined in equation (2), and

$$b_1 = 3K_0(c'_{ijkl0} + \Delta_{ijkl}) - 7c_{ijkl0}, \quad (9)$$

$$b_2 = 9K_0^2 c''_{ijkl0} + 3K'_0(b_1 + 7c_{ijkl0}) - 16b_1 - 49c_{ijkl0} \quad (10)$$

$$\text{and } \Delta_{ijkl} = -\delta_{ij}\delta_{kl} - \delta_{ik}\delta_{jl} - \delta_{il}\delta_{jk} \quad (11)$$

where c'_{ijkl0} and c''_{ijkl0} are the first and second derivative of c_{ijkl} , with respect to pressure. Δ_{ijkl} off-diagonal elastic constants (c_{iijj} in full tensor and c_{ij} in Voigt notation, with $i=1,2,3, i \neq j$), -1 for shear constants (c_{iiji} in full tensor notation with $i=1,2,3, i \neq j$ and c_{ij} in Voigt notation with $i=4,5,6, i=j$), and 0 otherwise. The isotropic bulk (K) and shear (G) moduli are determined using the relations

$$K_{\text{Voigt}} = (1/9)[c_{11} + c_{22} + c_{33} + 2(c_{12} + c_{13} + c_{23})], \quad (12)$$

$$K_{\text{Reuss}} = [s_{11} + s_{22} + s_{33} + 2(s_{12} + s_{13} + s_{23})]^{-1}, \quad (13)$$

$$G_{\text{Voigt}} = (1/15)[c_{11} + c_{22} + c_{33} - (c_{12} + c_{13} + c_{23}) + 3(c_{44} + c_{55} + c_{66})], \quad (14)$$

$$\text{and } G_{\text{Reuss}} = 15[4(s_{11} + s_{22} + s_{33} - (s_{12} + s_{13} + s_{23})) + 3(s_{44} + s_{55} + s_{66})]^{-1} \quad (15)$$

s_{ij} ($= c_{ij}^{-1}$) are the compliance tensor, *i.e.*, inverse of the elastic stiffness tensor (c_{ij}) and Voigt notation for the compliance tensor is used. Hill averages are estimated as average of Voigt and Reuss bounds (**Table 4, Figure 6**).

4. Discussion and Conclusion

Until the *first principles* result presented here the only available set of elastic constants for Phlogopite were those measured by (Alexandrov and Ryzhova, 1961) using ultrasonics at room pressure and later refined by (Alexandrov *et al.*, 1974). Two crystals were measured one from the Slyudyanka and other from Aldan region, near Lake Baikal, Russia. The experimental measurements were used to constrain the 5 independent elastic moduli with hexagonal symmetry rather than full 13 independent elastic moduli required for monoclinic symmetry of phlogopite. The refined experimental elastic constants (Alexandrov *et al.*, 1974) and the finite strain fit at 0 GPa for GGA and LDA results are shown in **Figure 5a**. The two crystals of Alexandrov *et al.*, 1974 are labeled, the values of the elastic constants of these two crystals agree very closely within 10 GPa despite the fact they come from regions that are separated by over 1000 km. The elastic constants from this study based on DFT agree with experimental values very closely within 15 GPa for c_{11} , c_{22} , c_{13} , c_{23} , c_{44} , c_{55} , and c_{66} for GGA. The predicted elastic constants for phlogopite using GGA are also similar to the

elastic constants for muscovite determined using Brillouin scattering (Vaughan and Guggenheim 1986) and ultrasonic method (Alexandrov and Ryzhova, 1961).

Phlogopite is a *tri*-octahedral mica, *i.e.*, all the three octahedral sites are occupied typically by a divalent cation (such as Mg^{2+}), whereas muscovite is a *di*-octahedral mica, where two of the three octahedral sites are occupied, typically by a trivalent cation (such as Al^{3+}). However, the remarkable similarity of the full elastic constant tensor between phlogopite and muscovite indicate that the elasticity is relatively insensitive of the exact chemistry of the octahedral sites.

Figure 5b-e shows the evolution of the elastic constants with pressure, the compressional elastic constants $c_{11} \sim c_{22} > c_{33}$ increase with pressure. The softer c_{33} indicates the high compressibility normal to the basal plane. The shear moduli with the relation $c_{44} \sim c_{55} < c_{66}$ do not increase significantly with pressure. The nearly equal compressional components $c_{11} \sim c_{22}$ and shear components $c_{44} \sim c_{55}$, are indications that the symmetry is close to hexagonal or transverse isotropic symmetry with quasi-isotropic behaviour in the basal plane. The pressure dependence of the off-diagonal elastic constants is more complex as they have compressional and shear contributions. Phlogopite has extremely anisotropic elastic properties, as shown by the *ab initio* monoclinic elastic constant tenors. The c^* -axis is significantly more compressible than the a - b plane as expected for a layer silicate.

The isotropic bulk and shear modulus stiffens for both GGA and LDA results based on *first principles* method (**Figure 6**). As a result the V_p and V_s also increases as a function of pressure. However, the pressure derivative for the shear modulus is lower than for the bulk modulus.

The seismic properties calculated using both the previous experimental and DFT based elastic constants illustrates the similarity in the results using the monoclinic and pseudo-hexagonal symmetry tensors (**Figure 7**), with high V_p and shear wave anisotropy in the basal plane. The monoclinic nature of phlogopite is reflected in the mirror symmetry plane (north-south direction in the stereo-plot, **Figure 7**) normal to the b -axis, which is most clearly seen on the S-wave anisotropy (AV_s) and V_{s1} polarization plots. Compared to the experimental elastic constants with pseudo-hexagonal symmetry, the anisotropy is lower by ~10% for V_p and ~20% for V_s for the DFT based elastic constants with monoclinic symmetry. This reflects the simplification of the velocity distribution introduced by the pseudo-hexagonal symmetry.

Upon compression both P- (AV_p) and S-wave (AV_s) anisotropy decreases (**Figure 8**). At room pressure the P-wave anisotropy (AV_p) is ~55% and (AV_s) S-wave ~77%. Upon compression up to ~11 GPa, these values decrease to 27% and 55%. Hydrous phases relevant at subduction zone settings, such as antigorite (serpentine polymorph), chlorite, and talc have extremely high P- (AV_p) S- wave (AV_s) anisotropy (**Figure 9**). At zero-pressure conditions, the talc has a maximum AV_p of 80 % and that of chlorite has a minimum AV_p of 30 %. At these conditions, the P-wave anisotropy, AV_p of antigorite, brucite, and phlogopite are quite similar. Upon compression beyond 5-6 GPa, *i.e.*, beyond the high-pressure stability of chlorite, talc, and antigorite, AV_p of phlogopite is maximum. At zero-pressure conditions, talc and phlogopite have the largest S-wave anisotropy with AV_s between 80-85 %. Upon compression, the AV_s of both talc and phlogopite reduces. However, the rate of reduction of talc is

significantly greater than that of phlogopite. In contrast, the AV_s of both chlorite and antigorite tends to increase upon compression. However, within the pressure stability region of chlorite and antigorite (*i.e.*, below 5 GPa), phlogopite has greater AV_s . Beyond the high pressure stability region of chlorite and antigorite ($P > 6$ GPa), AV_s of chlorite and antigorite are greater than that of phlogopite, however these phases are unlikely to be stable. Hence, AV_s of phlogopite is likely to play a dominant role.

Owing to the wide range of pressure-temperature stability, *i.e.*, pressures up to 9 GPa and temperatures up to 1400 °C (Trønnes, 2002), Phlogopite micas could occur at wide variety of settings such as in upper mantle with normal mantle geotherm and subduction zone settings. Phlogopite rich bearing ultrapotassic MARID type of rocks (up to 90 % phlogopite) have been reported as nodules in kimberlites from continental cratons (Waters, 1987). These phlogopite bearing MARID rocks may occur at the lithosphere asthenosphere boundary (LAB), which is characterized by intense metasomatism (O'Reilly and Griffin, 2010). If the mantle flow beneath the LAB is essentially horizontal, *i.e.*, parallel to the LAB then the MARID rocks with large modal fractions of phlogopite is likely to orient its (001) horizontal layers parallel to the LAB. The resulting vertical V_p is likely to be slow and the S-wave anisotropy AV_s is likely to be low. Reduction in velocity and loss of anisotropy is often observed across the LAB settings (Eaton *et al.*, 2009). The presence of melt is likely to reinforce the velocity reduction.

The subduction zone settings are likely to be characterized by significant hydration and thus stabilizing variety of hydrous phases including phlogopite.

The anisotropy of the layered hydrous silicates such as talc (Stixrude, 2002; Mainprice *et al.*, 2008) and antigorite (Bezacier *et al.*, 2010; Mookherjee and Capitani, 2011) are significantly larger than the major mantle phases such as olivine. In certain subduction zones such as Rykyu, in addition to the trench parallel shear wave polarization anisotropy, a large delay time has been observed (Long and Silver, 2008). To explain such a large delay time of around 1-2 s with a peridotitic rock dominated by olivine, one would require a significant thickness of around ~100- 150 km. Owing to the large anisotropy layered silicates are plausible candidates (Katayama *et al.*, 2009; Bezacier *et al.*, 2010; Mookherjee and Capitani, 2011). Although layered hydrous silicate minerals tend to have similar crystal preferred orientations due to the very strong control of their layered structure. Typical CPO pattern is a strong alignment of the basal plane with foliation plane of the rock and the weak alignment of *a*- or *b*-directions may also occur in the foliation plane. This has been observed in series of earlier studies (Katayama *et al.*, 2009, Lloyd *et al.*, 2009, Jung, 2011, Padron-Navarta *et al.*, 2012). To our knowledge, at present, experimental study of slip systems of phlogopite is lacking. The elastic anisotropy is also dominated by very strong control of the layered structure as illustrated by the similarity between muscovite and phlogopite. Based on these arguments on the deformation fabric, together with the seismic-anisotropy, a modest 10-15 km thick layer could explain both the trench parallel shear wave polarization anisotropy and a large delay time.

The mantle wedge in the subduction zone settings are characterized by a V_p/V_s ratio ranging between 1.76 and 1.82 (Zhang *et al.*, 2004, Syracuse *et al.*, 2008; Tsuji *et al.*, 2008). Recent high-resolution measurement of seismic

velocities in subduction zone settings have revealed unusually low V_p / V_s ratios ranging from 1.65 to 1.72 (Wagner *et al.*, 2005, 2006, 2008; Rossi *et al.*, 2006; Eberhart-Phillips *et al.*, 2006). A unique combination of ray path and anisotropy is required to explain such unusual V_p / V_s ratios. It is known that the mantle wedge is severely altered owing to release of fluids from dehydrating minerals in the subducting slabs. Although, fluids tend to stabilize layered hydrous silicate phases such as antigorite, chlorite, and phlogopite, these layered minerals typically have an isotropic $V_p / V_s \sim 2.0$. Olivine, the dominant mantle mineral may explain such an unusual $V_p / V_s \sim 1.65$ to 1.72 when [100] axis of olivine is oriented perpendicular to rather than parallel to the ray path (Hacker and Abers, 2012). We find that the anisotropy of the phlogopite at a density of ~ 2.79 gm/cm³ is such that the V_p/V_{S1} ratios are as low as 1.5 (**Figure 10**) and hence these hydrous phases such as phlogopite could also explain the unusual V_p / V_s ratios, in addition to the dominant peridotitic rocks.

Acknowledgements:

MM is supported by the US National Science Foundation grant (EAR-1250477). MM acknowledges computing resources (request # EAR130015) from the Extreme Science and Engineering Discovery Environment (XSEDE), which is supported by National Science Foundation grant number OCI-1053575. GM acknowledges funding from the French PNP program (INSU-CNRS).

References

- Alexandrov, K. S., Ryzhova, T. V., 1961. Elastic properties of rock-forming minerals. II. Layered Silicates. Bulletin of the Academy of Sciences of the U.S.S.R., Geophysical Series, 9, 1165-1168.
- Aleksandrov, K. S., Alchikov, U. V., Belikov, B. P., Zaslavskii, B. I. & Krupnyi, A. I. 1974. Velocities of elastic waves in minerals at atmospheric pressure and increasing precision of elastic constants by means of EVM (in Russian). Izvestiya of the Academy of the Sciences of the USSR, Geologic Series, 10, 15-24.
- Bailey, D. K., 1982. Mantle metasomatism – continuing chemical change within the earth. *Nature*, 296, 525-550.
- Bezacier, L., Reynard, B., Bass, J. D., Sanchez-Valle, C., Van de Moortele, B., 2010. Elasticity of antigorite, seismic detection of serpentinites, and anisotropy in subduction zones. *Earth and Planetary Science Letters*, 289, 198-208.
- Birch, F., 1978. Finite strain isotherm and velocities for single-crystal and polycrystalline NaCl at high pressures and 300 K. *Journal of Geophysical Research*, 83, 1257-1268.
- Ceperley, D.M., and Adler, B.J. (1980) Ground state of the electron gas by a stochastic method. *Physical Review Letters*, 45, 566-569.
- Chantel, J., Mookherjee, M., Frost, D. J., 2012. The elasticity of lawsonite at high pressure and the origin of the low velocity layers in subduction zones. *Earth and Planetary Science Letters*, 349-350, 116-125.
- Chon, C. M., Lee, C. K., Song, Y., Kim, S. A., 2006. Structural changes and oxidation of ferroan phlogopite with increasing temperature: in situ neutron

- powder diffraction and Fourier transform infrared spectroscopy. *Physics and Chemistry of Minerals*, 33, 289–299.
- Comodi, P., Fumagalli, P., Montagnoli, M., Zanazzi, P. F., 2004. A single-crystal study on the pressure behavior of phlogopite and petrological implications. *American Mineralogist*, 89, 647-653.
- Davies, G. F., 1974. Effective elastic-moduli under hydrostatic stress. 1. Quasi-harmonic theory. *Journal of the Physics and Chemistry of Solids*, 35, 1513-1520.
- Eaton, D. W., Darbyshire, F., Evans, R. L., Grütter, H., Jones, A. G., Yuan, X., 2009. The elusive lithosphere-asthenosphere boundary (LAB) beneath cratons. *Lithos*, 109, 1-22.
- Eberhart-Phillips, D., Christensen, D. H., Brocher, T. M., Hansen, R., Rupert, N. A., Haeussler, P. J., Abers, G. A., 2006. Imaging the transition from Aleutian subduction to Yakutat collision in central Alaska, with local earthquakes and active source data. *Journal of Geophysical Research*, 111, B11303.
- Fumagalli, P. Stixrude, L. 2007. The 10 Angstrom phase at high pressure by first principles calculations and implications for the petrology of subduction zones. *Earth and Planetary Science Letters*, 260, 212-226.
- Fumagalli, P., Zanchetta, S., Poli, S., 2009. Alkali in phlogopite and amphibole and their effects on phase relations in metasomatized peridotites: a high-pressure study. *Contributions to Mineralogy and Petrology*, 158, 723–737.
doi: 0.1007/s00410-009-0407-4
- Gatta, G. D., Merlini, M., Rotiroti, N., Curetti, N., Pavese, A., 2011. On the crystal chemistry and elastic behavior of a phlogopite 3T. *Physics and Chemistry of Minerals*, 38, 655–664. doi: 007/s00269-011-0438-z.

- Hacker, B. R., Abers, G. A., 2012. Subduction Factory 5: Unusually low Poisson's ratios in subduction zones from elastic anisotropy of peridotite. *Journal of Geophysical Research*, 117, B06308.
- Hamann, D. R., 1997. H₂O hydrogen bonding in density functional theory. *Physical Review B*, 55, R10157-R10160.
- Hernandez-Haro, N., Ortega-Castro, J., Del Valle, C. P., Munoz-Santiburico, D., Sainz-Diaz, C. I., Hernandez-Laguna, A., 2013. Computational study of the elastic behavior of the 2M₁ muscovite-paragonite series. *American Mineralogist*, 98, 651-664.
- Hazen, R. M., Finger, L. W., 1978. The crystal structures and compressibilities of layer minerals at high pressure. II. Phlogopite and chlorite. *American Mineralogist*, 63, 293-296.
- Hohenberg, P., Kohn, W., 1964. Inhomogenous electron gas. *Physical Review B*, 136, B864-871.
- Jiang, F., Speziale, S., Duffy, T. S., 2006. Single-crystal elasticity of brucite, Mg(OH)₂, to 15 GPa by Brillouin scattering. *American Mineralogist*, 91, 1893-1900.
- Jung, H., 2011. Seismic anisotropy produced by serpentine in mantle wedge. *Earth and Planetary Science Letters*, 307, 535-543.
- Karki, B. B., Stixrude, L., Wentzcovitch, R. M., 2001. Elastic properties of major mantle materials of earth's mantle from first principles. *Reviews of Geophysics*, 39, 507-534.
- Katayama, I., Hirauchi, K.-I., Michibayashi, K., Ando, J.-I., 2009. Trench-parallel anisotropy produced by serpentine deformation in hydrated mantle wedge. *Nature*, 461, 1114-1117.

- Kohn, W., Sham, L. J., 1965. Self-Consistent Equations Including Exchange and Correlation Effects. *Physical Review* 140, 1133-1138.
- Kenzett, J., Ulmer, P., 1999. The stability of hydrous potassic phases in lherzolitic mantle- an experimental study to 9.5 GPa in simplified and natural bulk compositions. *Journal of Petrology*, 40, 629-652.
- Kresse, G., Furthmuller, J., 1996a. Efficiency of ab-initio total energy calculations for metals and semiconductors using a plane-wave basis set. *Computational Materials Science*, 6, 15-50.
- Kresse, G., Furthmuller, J., 1996b. Efficient iterative schemes for ab initio total-energy calculations using a plane-wave basis set. *Physical Review B* 54, 11169-11186.
- Kresse, G., Hafner, J., 1993. Ab initio Molecular-Dynamics for Liquid-Metals. *Physical Review B* 47, 558-561.
- Kresse, G., Joubert, D. 1999. From ultrasoft pseudopotentials to the projector augmented-wave method. *Physical Review B* 59, 1758-1775.
- Kushiro, I., Akimoto, S., Syono, Y., 1967. Stability of phlogopite at high pressures and possible presence of phlogopite in the earth's upper mantle. *Earth and planetary science letters*, 3, 197-203.
- Lloyd, G. E., Butler, R. W. H., Casey, M., Mainprice, D., 2009. Mica, deformation fabrics and the seismic properties of the continental crust. *Earth and Planetary Science Letters*, 288, 320-328.
- Long, M. D., Silver, P. G., 2008. The subduction zone flow field from seismic anisotropy. *Science*, 319, 315-318.
- Mainprice, D., 1990. A fortran program to calculate seismic anisotropy from the lattice preferred orientation of minerals. *Computers and Geosciences* 16,

385-393.

- Mainprice, D., Le Page, Y., Rodgers, J., Jouanna, P., 2008. Ab initio elastic properties of talc from 0 to 12 GPa: interpretation of seismic velocities at mantle pressures and prediction of auxetic behavior at low pressure. *Earth and Planetary Science Letters*, 274, 327-338.
- Mainprice, D., Ildefonse, B., 2009. Seismic anisotropy of subduction zone minerals - contribution of hydrous phases. Springer series 'Frontiers in Earth Sciences' Subduction Zone Dynamics Edited by Serge Lallemand and Francesca Funiciello doi 10.1007/978-3-540-87974-9.
- Meade, C., Jeanloz, R., 1990. Static compression of Ca(OH)₂ at room temperature: observations of amorphization and equation of state measurements to 10.7 GPa. *Geophysical Research Letters*, 17, 1157-1160.
- Militzer, B., Wenk, H.-R., Stackhouse, S., Stixrude, L., 2011. First-principles calculation of the elastic moduli of sheet silicates and their application to shale anisotropy. *American Mineralogist*, 96, 125-137.
- Monkhorst, H. J., Pack, J. D., 1976. Special points for Brillouin-zone integrations. *Physical Review B* 13, 5188-5192.
- Mookherjee, M., Redfern, S. A. T., Zhang, M., 2001. Thermal response of structure and hydroxyl ion of phengite- 2M₁: an in situ neutron diffraction and FTIR study. *European Journal of Mineralogy*, 13, 545-555.
- Mookherjee, M., Redfern, S. A. T., 2002. A high-temperature Fourier transform infrared study of the interlayer and Si-O stretching region in phengite 2M₁. *Clay Minerals*, 37, 323-336.
- Mookherjee, M., Stixrude, L., 2006. High-pressure proton disorder in brucite. *American Mineralogist*, 91, 127-134.

- Mookherjee, M., Stixrude, L., 2009. Structure and elasticity of serpentine at high-pressure. *Earth and Planetary Science Letters*, 279, 11-19.
- Mookherjee, M., Capitani, G. C., 2011. Trench parallel anisotropy and large delay times: Elasticity and anisotropy of antigorite at high pressures. *Geophysical Research Letters*, 38, L09315, doi: 10.1029/2011GL047160.
- Mookherjee, M., Bezacier, L., 2012. The low-velocity layer in subduction zone: structure and elasticity of glaucophane at high pressures. *Physics of the Earth and Planetary Interiors*, 208-209, 50-58.
- Mookherjee, M., Mainprice, D., 2014. Unusually large shear wave anisotropy for chlorite in subduction zone settings. *Geophysical Research Letters*, 41, doi:10.1002/2014GL059334.
- Nye, J. F., 1985. Physical properties of crystals, Oxford University Press, Clarendon.
- Oganov, A. R., Brodholt, J. P., Price, G. D., 2002. Ab initio theory of thermo-elasticity and phase transitions in minerals. *Energy Modelling in Minerals*, European Mineralogical Union Notes in Mineralogy V.4 edited by Gramaccioli, C.M., 83-170.
- O'Reilly, S. Y., Griffin, W. L., 2010. The continental lithosphere-asthenosphere boundary: Can we sample it? *Lithos*, 120, 1-13.
- Ortega-Castro, J., Hernandez-Haro, N., Timon, V., Sainz-Diaz, C. I., Hernandez-Laguna, A., 2010. High-pressure behavior of 2M₁ muscovite. *American Mineralogist*, 95, 249-259.
- Padron-Navarta, J. A., Tommasi, A., Garrido, C. J., Sanchez-Vizcaino, V. L., 2012. Plastic deformation and development of antigorite crystal preferred

- orientation in high-pressure serpentinites. *Earth and Planetary Science Letters*, 349-350, 75-86.
- Pavese, A., Levy, D., Curetti, N., Diella, V., Fumagalli, P., Sani, A., 2003. Equation of state and compressibility of phlogopite by in-situ high-pressure X-ray powder diffraction. *European Journal of Mineralogy*, 15, 455-463.
- Perdew, J.P., Wang, Y., 1986. Accurate and simple density functional for the electronic exchange energy: Generalized gradient approximation. *Physical Review B*, 33, 8800-8802.
- Perdew, J.P., Chevary, J.A., Vosko, S.H., Jackson, K.A., Pederson, M.R., Singh, D.J., Fiolhais, C., 1991. Atoms, molecules, solids, and surfaces: Applications of the generalized gradient approximation for exchange and correlation. *Physical Review B*, 46, 6671-6687.
- Perdew, J. P., Burke, K., Erzerhof, M. 1996. Generalized gradient approximation made simple. *Physical Review Letters*, 77, 3865-3868.
- Rayner, J. H., 1974. The crystal structure of phlogopite by neutron diffraction. *Mineralogical magazine*, 39, 850-856.
- Redhammer, G. J., Roth, G., 2002. Single-crystal refinements and crystal chemistry of synthetic trioctahedral micas $KM_3(Al^{3+}, Si^{4+})_4O_{10}(OH)_2$, where $M = Ni^{2+}, Co^{2+}, Fe^{2+}$, or Al^{3+} . *American Mineralogist*, 87, 1464-1476.
- Rossi, G., Abers, G., Rondenay, S., Chiristensen, D. H., 2006. Unusual mantle Poission's ratio, subduction, and crustal structure in central Alaska. *Journal of Geophysical Research*, 111, B09311.
- Sato, K., Katsura, T., Ito, E., 1996. Phase relations of phlogopite with and without enstatite up to 8 GPa : implication to potassic magmatism and mantle metasomatism. *Technical Report of ISEI Ser. A*, No. 65.

- Sato, K., Katsura, T., Ito, E., 1997. Phase relations of natural phlogopite with and without enstatite up to 8 GPa: implication for mantle metasomatism. *Earth and Planetary Science Letters*, 146, 511-526.
- Sekine, T., Wyllie, P. J., 1982. Phase relationships in the system KAISiO₄-Mg₂SiO₄-SiO₂-H₂O as a model or hybridization between hydrous siliceous melts and Peridotite. *Contributions to Mineralogy and Petrology*, 79, 368-374. doi: 0010-7999/82/0079/0368.
- Smyth, J. R., S. D. Jacobsen, Swope, R. J., Angel, R. J., Arlt, T., Domanik, K., Holloway, J. R., 2000. Crystal Structures and compressibilities of synthetic 2M₁ and 3T phengite micas. *European Journal of Mineralogy*, 12, 955-963.
- Stackhouse, S., Coveney, P. V., Benoit, D. M., 2004. Density functional theory based study of the dehydroxylation behavior of aluminous dioctahedral 2:1 layer type clay minerals. *Journal of Physical Chemistry B* 108, 9685-9694.
- Stixrude, L., 2002. Talc under tension and compression: spinodal instability and structure at high pressure. *Journal of Geophysical Research*, 107, B 001684.
- Stixrude, L., Peacor, D. R., 2002. First principles study of illite-smectite and implications for clay mineral systems. *Nature*, 420, 165-168.
- Sudo, A., Tatsumi, Y., 1990. Phlogopite and K-amphibole in the upper mantle: implication for magma genesis in subduction zones. *Geophysical Research Letters*, 17, 29-32. doi: 0094-8276/90/89GL-0336.
- Sweeney, R. J., Thompson, A. B., Ulmer P., 1993. Phase relations of a natural MARID composition and implications for MARID genesis, lithospheric

- melting and mantle metasomatism. Contributions to Mineralogy and Petrology, 115, 225-241.
- Syracuse, E. M., Abers, G. A., Fischer, K., MacKenzie, L., Rychert, C., Protti, M., Gonzalez, V., Strauch, W., 2008. Seismic tomography and earthquake locations in the Nicaraguan and Costa Rican upper mantle. Geochemistry Geophysics Geosystems, 9, Q07S08.
- Thompson, A. B., 1992. Water in the Earth's upper mantle. Nature, 358, 295-302.
- Trønnes, R. G., 2002. Stability range and decomposition of potassic richterite and phlogopite end members at 5-15 GPa. Mineralogy and Petrology, 74, 129-148.
- Tsuchiya, J., Tsuchiya, T., Tsuneyuki, S., 2005. First-principles study of hydrogen bond symmetrization of phase D under high pressure. American Mineralogist, 90, 44-49.
- Tsuchiya, J., Tsuchiya, T., Wentzcovitch, R. M., 2008. Vibrational properties of δ -AlOOH under pressure. American Mineralogist, 93, 477-482.
- Tsuchiya, J., Tsuchiya, T., 2009. Elastic properties of δ -AlOOH under pressure-first principle investigation. Physics of the Earth and planetary interiors, 174, 122-127.
- Tsuji, Y., Nakajima, J., Hasegawa, A., 2008. Tomographic evidence for hydrated oceanic crust of the Pacific slab beneath northeastern Japan: Implication for water transportation in subduction zones. Geophysical Research Letter, 35, L14308.
- Vaughan, M. T., Guggenheim, S., 1986. Elasticity of muscovite and its relationship to crystal structure. Journal of Geophysical Research, 91, 4657-4664.

- Wagner, L. S., Beck, S. L., Zandt, G., 2005. Upper mantle structure in the south central Chilean subduction zone (30° to 36°S). *Journal of Geophysical Research*, 110, B01308.
- Wagner, L. S., Beck, S. L., Zandt, G., Ducea, M., 2006. Depleted lithosphere, cold, trapped asthenosphere, and frozen melt puddles above the flat slab in central Chile and Argentina. *Earth and Planetary Sciences Letters*, 245, 289-301.
- Wagner, L. S., Anderson, M. L., Jackson, J., Beck, S. L., Zandt, G., 2008. Seismic evidence for orthopyroxene enrichment in the continental lithosphere. *Geology*, 36, 935-938.
- Waters, F. G., 1987. A suggested origin of MARID xenoliths in kimberlites by high-pressure crystallization of an ultrapotassic rock such as lamproite. *Contribution to Mineralogy and Petrology*, 95, 523-533.
- Weaver, J. S., 1976. Application of finite strain theory to non-cubic crystals. *Journal of the Physics and Chemistry of Solids*, 37, 711-718.
- Wyllie, P. J., Sekine, T., 1982. The Formation of Mantle Phlogopite in Subduction Zone Hybridization. *Contributions to Mineralogy and Petrology*, 79, 375-380. doi: 0010-7999/82/0079/0375.
- Yoder, H. S., Eugster, H. P., 1954. Phlogopite synthesis and stability range. *Geochimica et Cosmochimica Acta*, 6, 167-185.
- Yoder, H. S., Kushiro, I., 1969. Melting of a hydrous phase: phlogopite. *American Journal of Science*, 267-A, 558-583.
- Zhang, H., Thurber, C. H., Shelly, D., Ide, S., Beroza, G. C., Hasegawa, A., 2004. High-resolution subducting slab structure beneath northern Honshu, Japan, revealed by double-difference tomography. *Geology*, 32, 361-364.

Figure Captions

Figure 1. Crystal structure of phlogopite with $C2/m$ space group symmetry. TO_4 tetrahedral units where $T = \text{Si}, \text{Al}$ are arranged to form *di*-trigonal rings. Two such tetrahedral sheets with their tetrahedral apex pointing towards each other sandwich an octahedral layer. MO_6 octahedral units are indicated by light yellow color where $M = \text{Mg}$. Interlayer region is occupied by potassium atoms. The silicon (Si) and aluminum (Al) atoms are shown as dark and light blue spheres respectively. The potassium (K) atoms are shown as purple large spheres. The hydrogen atoms are denoted as white sphere; the oxygen atoms are denoted as red spheres.

Figure 2. (a) Plot of energy with respect to unit-cell volume predicted by *first principles*. Legend: LDA- red symbols; GGA- blue symbols. (b) Plot of pressure vs. unit-cell volume. Experimental results- x-ray diffraction data are denoted by ‘grey’ (C- Comodi et. al. 2004) and ‘white’ symbols (P- Pavese et. al., 2003). *First principles* result from LDA (red symbols) and GGA (blue symbols) tend to bracket the experimental results.

Figure 3. Plot of the lattice parameters vs. pressure (a) *a*-axis, (b) *b*-axis, and (c) *c*-axis. Inset in the panel (c) also shows the plot of lattice parameter β vs. pressure. In panels (d-f), linear normalized pressure, F_l vs. the linear Eulerian finite strain, f_l are plotted for *a*-axis, *b*-axis, and *c**-axis. The intercept along the ordinate indicates the linear compressibility K_a , K_b and K_c . Data from previous x-ray diffraction studies are denoted by ‘white’ (C- Comodi et. al., 2004) and ‘grey’ (P-Pavese et. al., 2003) symbols. The *first principle* simulation results from this study are denoted by ‘red’ (LDA) and ‘blue’ (GGA) symbols.

Figure 4. Plot of volume of polyhedral units vs. pressures- **(a)** tetrahedral units TO_4 are represented in the right-ordinate axis; the octahedral units MO_6 are represented in the left-ordinate axis; **(b)** the interlayer with 12 fold coordination (KO_{12}) vs. pressure. The first principle simulations with LDA and GGA are shown in ‘red’ and ‘blue’ symbols respectively. The simulation results tend to bracket the experimental results; **(c)** Plot of α vs. pressure. The α angle characterizes the in-plane rotation of tetrahedral units as shown in the inset- a perfect hexagon, shown in dashed line, the angle between consecutive oxygen atoms would be 120° and hence $\alpha = 0^\circ$. In contrast, for a *di*-trigonal ring of tetrahedral units, the angle between consecutive oxygen atoms is either greater than or less than 120° resulting in $\alpha > 0^\circ$. Under compression the *di*-trigonal distortion characterized by α , increases with pressure. The first principle simulations with LDA and GGA are shown in ‘red’ and ‘blue’ symbols respectively. Data from previous x-ray diffraction studies are denoted by ‘grey’ (C- Comodi et. al., 2004). **(d)** Plot of O-H, O---H and O----O distances with pressure. Within the compression range explored in this study there is no evidence for the formation of hydrogen bonds since O-H bond distances remain rather constant and do not increase in length, which is often diagnostic of hydrogen bonding.

Figure 5. **(a)** Comparison between experimental results and *ab initio* predicted elastic constants at room pressure. Experimental elastic tensor for two distinct phlogopite samples A and B (A1974) (Alexandrov *et al.*, 1974) are compared with the results from this study. We also compare phlogopite single crystal elastic constants with muscovite. Muscovite single crystal

elastic constant data are from VG1986 (Vaughan and Guggenheim, 1986); AR1961 (Alexandrov and Ryzhova, 1961). Elastic constants, c_{ij} as a function of pressure- **(b)** compressional components, c_{11} , c_{22} and c_{33} ; **(c)** off-diagonal components, c_{12} , c_{13} , and c_{23} ; **(d)** off-diagonal components, c_{15} , c_{25} , and c_{35} ; **(e)** shear components, c_{44} , c_{55} , c_{46} , and c_{66} . The 'blue' and 'red' filled symbols from *first principle* simulation with GGA and LDA respectively.

Figure 6. **(a)** Plot of bulk and shear modulus vs. pressure. Both Voigt and Reuss bounds are shown. **(b)** Plot of compressional (V_p), shear (V_s) sound velocity vs. pressure. The 'blue' and 'red' filled symbols from *first principle* simulation with GGA and LDA respectively.

Figure 7. Stereo plot of *Ab initio* predicted seismic anisotropy at 0 GPa: AV_p , $AV_s\%$ and V_{s1} polarization for GGA, LDA methods (this study), also shown are plots from the elastic constants from previous experiments (Alexandrov *et al.*, 1974).

Figure 8. Plot of seismic anisotropy for phlogopite, **(a)** AV_p and $AV_s\%$ **(b)** AV_{s1} , AV_{s2} , AV_p/V_{s1} , and AV_p/V_{s2} as a function of pressure

Figure 9. Plot of **(a)** P-wave anisotropy, AV_p and **(b)** S-wave anisotropy, AV_s for various hydrous phases relevant for the subduction zone settings, as a function of pressure. Mineral abbreviations: chl- chlorite (Mookherjee and Mainprice, 2014), ant- antigorite- serpentine polymorph (Mookherjee and Capitani, 2011), tlc- talc (Mainprice *et al.*, 2008), bru- brucite (Jiang *et al.*, 2006). The light green shaded area represents the high-pressure stability field of antigorite, chlorite, and talc (Mainprice and Ildefonse, 2009 and

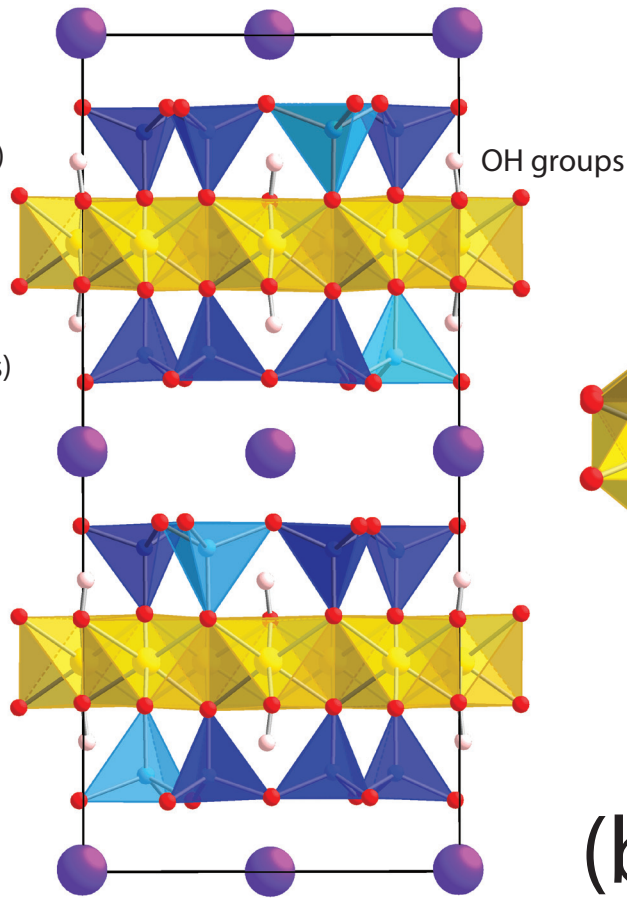
references therein), the light purple shaded area represents the high-pressure stability field for phlogopite (Trønnes, 2002).

Figure 10. (a) Variation of compressional (V_P), shear (V_S) sound velocity as a function of orientation with respect to the [001] direction. (b) Plot of delay time/layer thickness [$\delta V_S / (V_{S1} \times V_{S2})$] as a function of as a function of the angle of incidence between the seismic ray path and (001) plane of phlogopite. In the top, the layered hydrous silicates with the stacking of (001) planes are shown with the seismic rays oriented nearly perpendicular, i.e., seismic rays are almost aligned with the [001] direction. Also shown are the stacking of (001) planes and seismic rays are almost aligned with plane i.e., nearly perpendicular to the [001] direction. (c) Plot of V_P/V_S ratio as a function of V_S for phlogopite at a density of 2.79 gm/cm³. Since there is significant anisotropy the P-wave and S-wave (V_{S1} ; V_{S2}) for all propagation directions are plotted, the spread in the V_P/V_{S1} and V_P/V_{S2} results from the large anisotropy. Also shown is the isotropic V_P/V_S (filled red symbol). Two region marked as ‘usual, observed’ (grey) and ‘unusual, observed’ (red) represents the seismological observations in mantle wedges (*modified from* Hacker and Abers, 2012). Once the anisotropy of hydrous phases are taken into account, the hydrous phases such as phlogopite could readily explain the unusual observations of V_P/V_S in subduction zones.

(a)

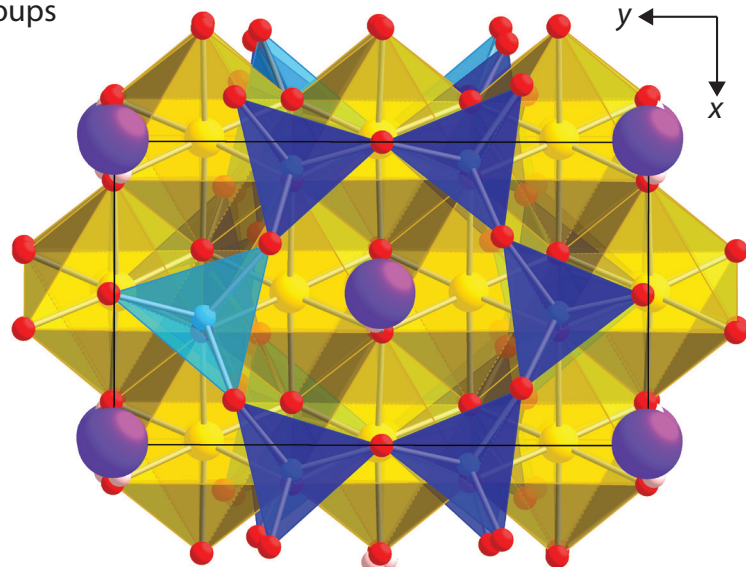
T-tetrahedral layer
(SiO_4 and AlO_4 units)
O-octahedral layer
(MgO_6 units)
T-tetrahedral layer
(SiO_4 and AlO_4 units)
Interlayer
(potassium ion, K)

y ←
z ↓



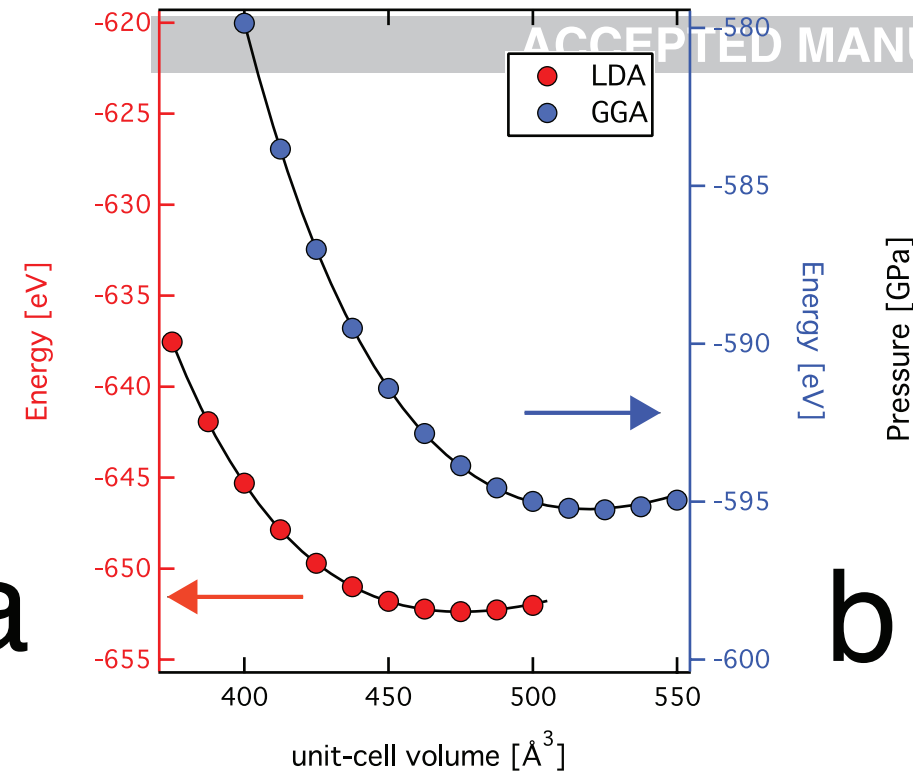
PT

(b)

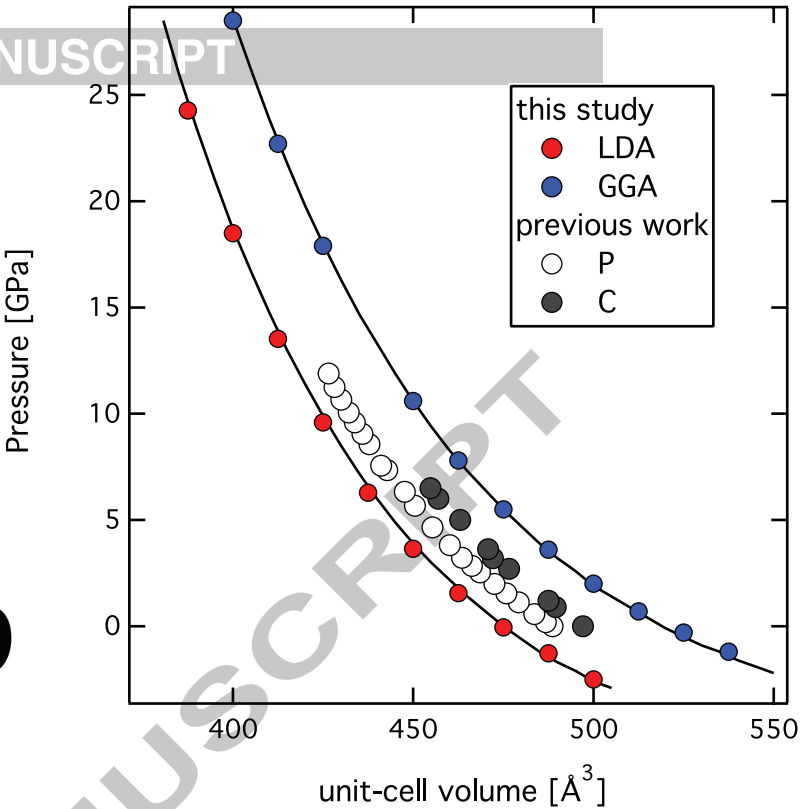


SiO_4 and AlO_4 units form
di-trigonal rings

ACCEPTED MANUSCRIPT



b



lattice parameter [Å]

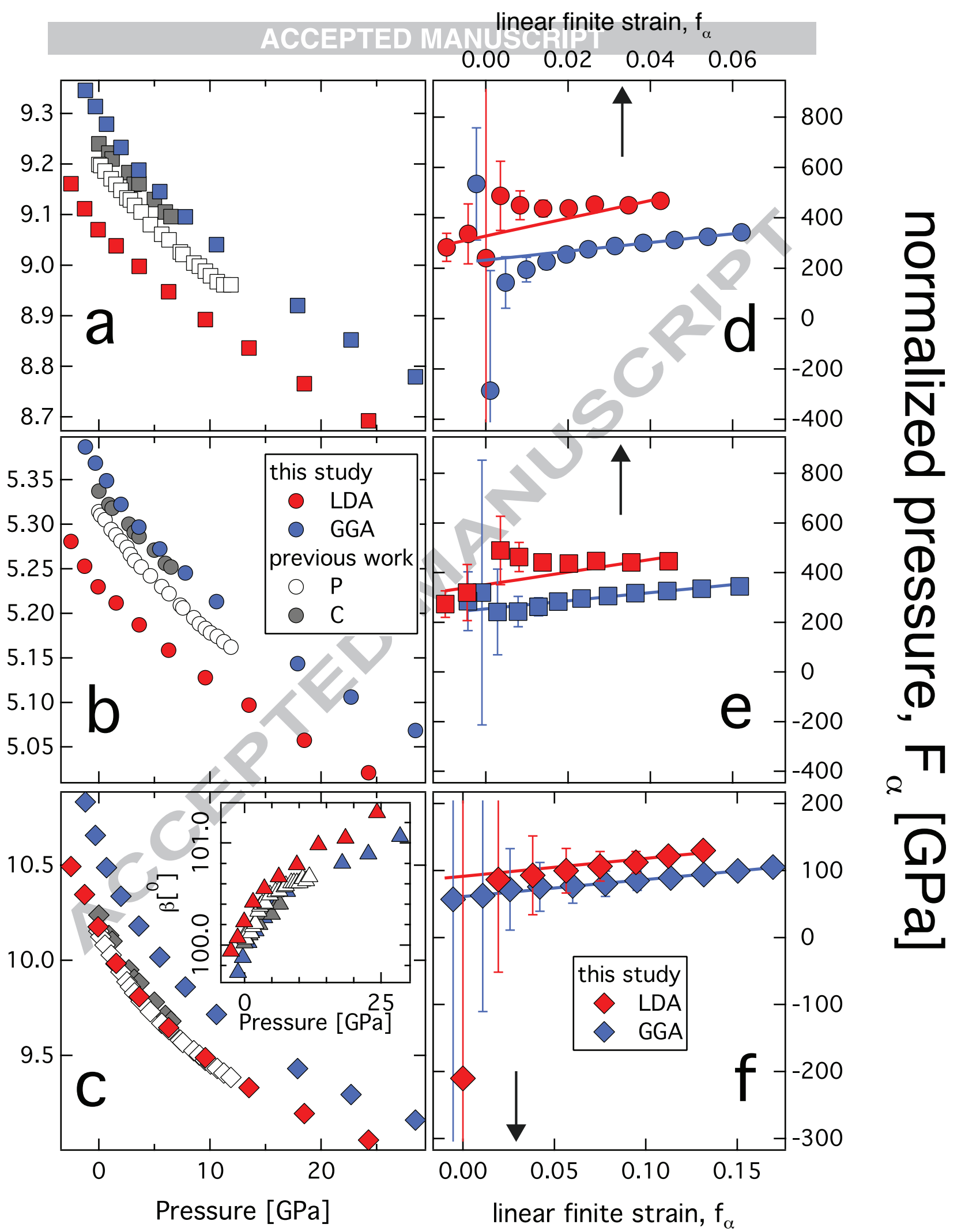
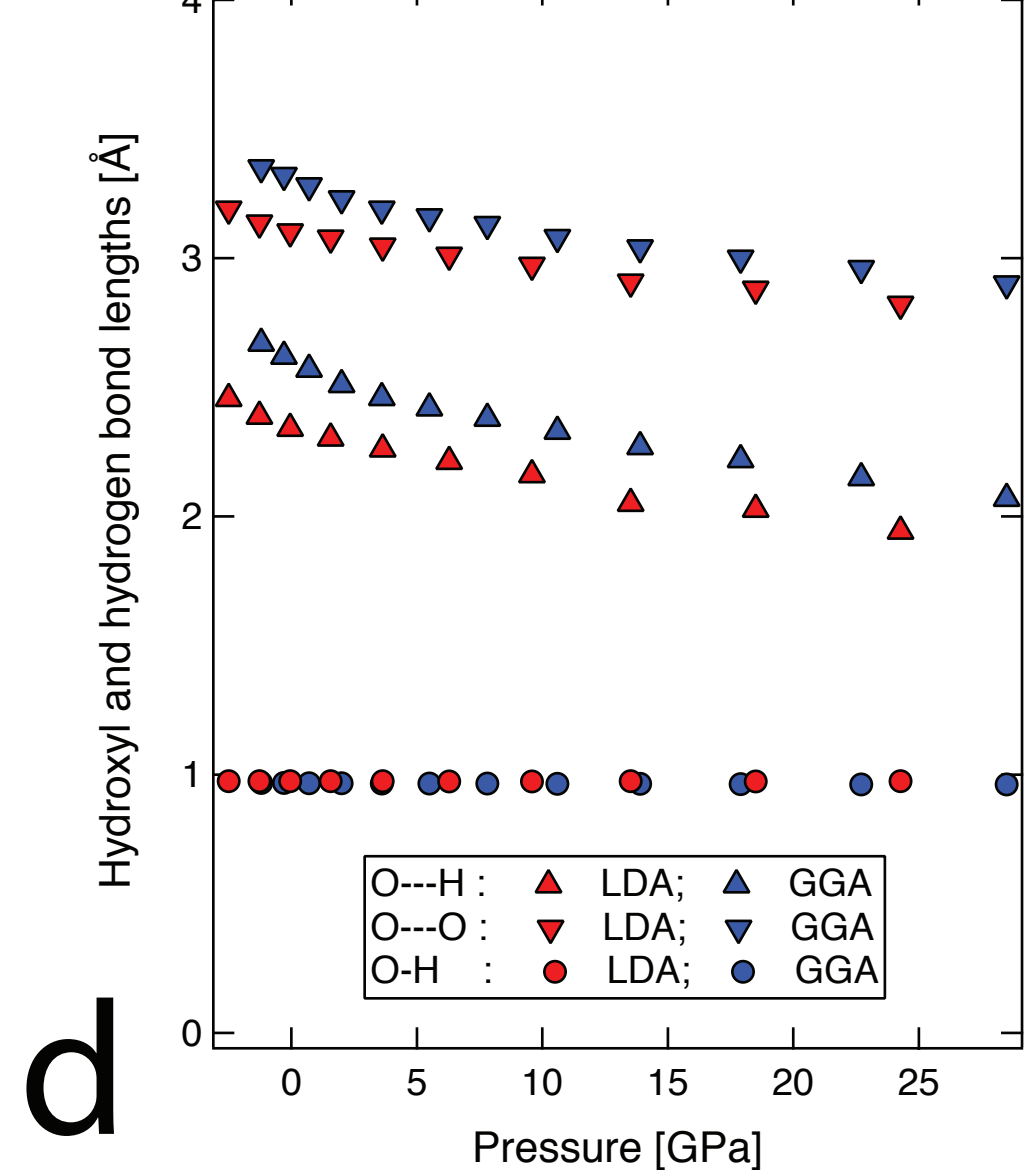
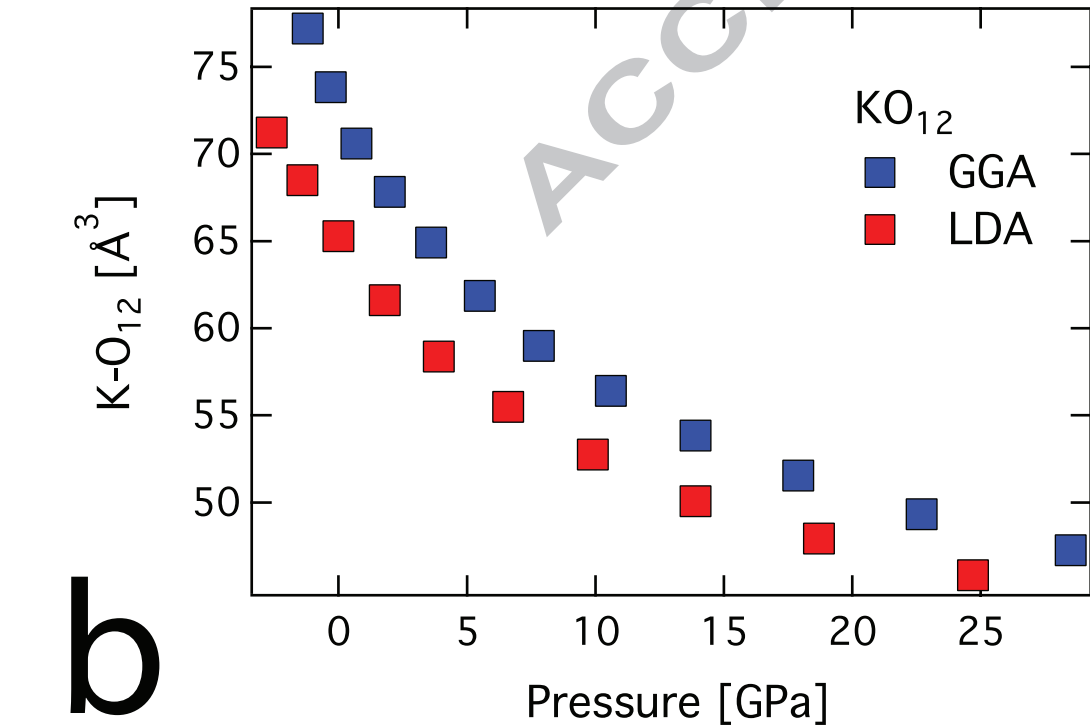
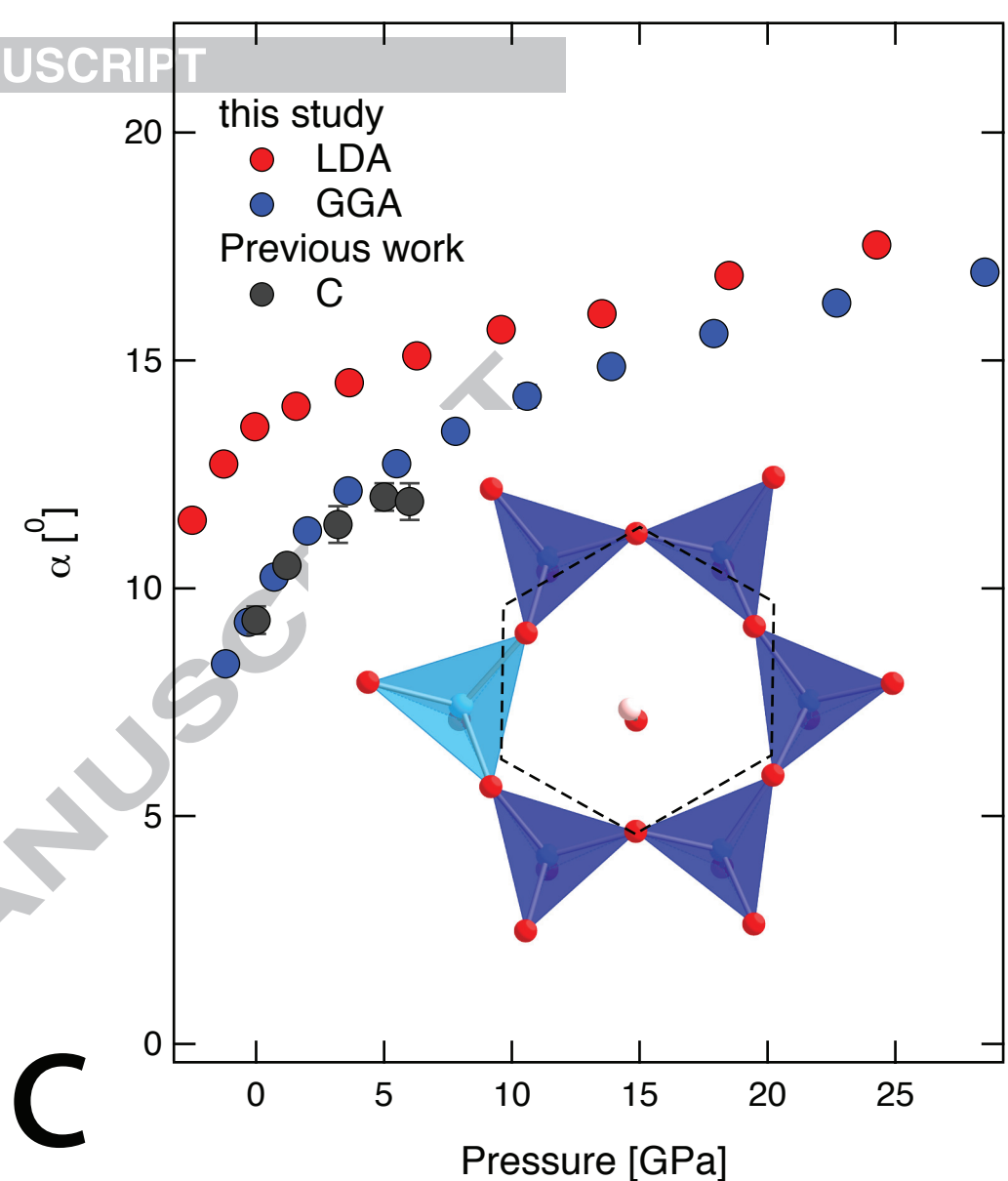
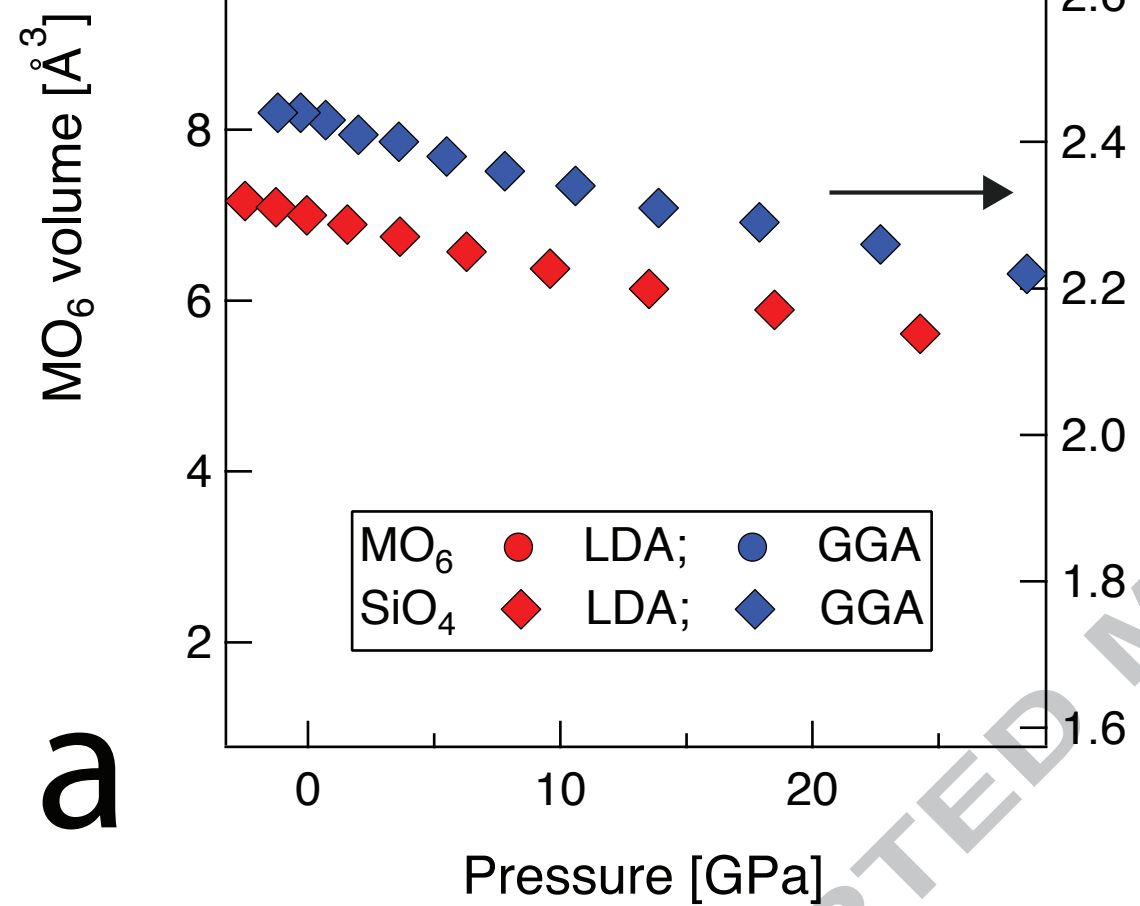
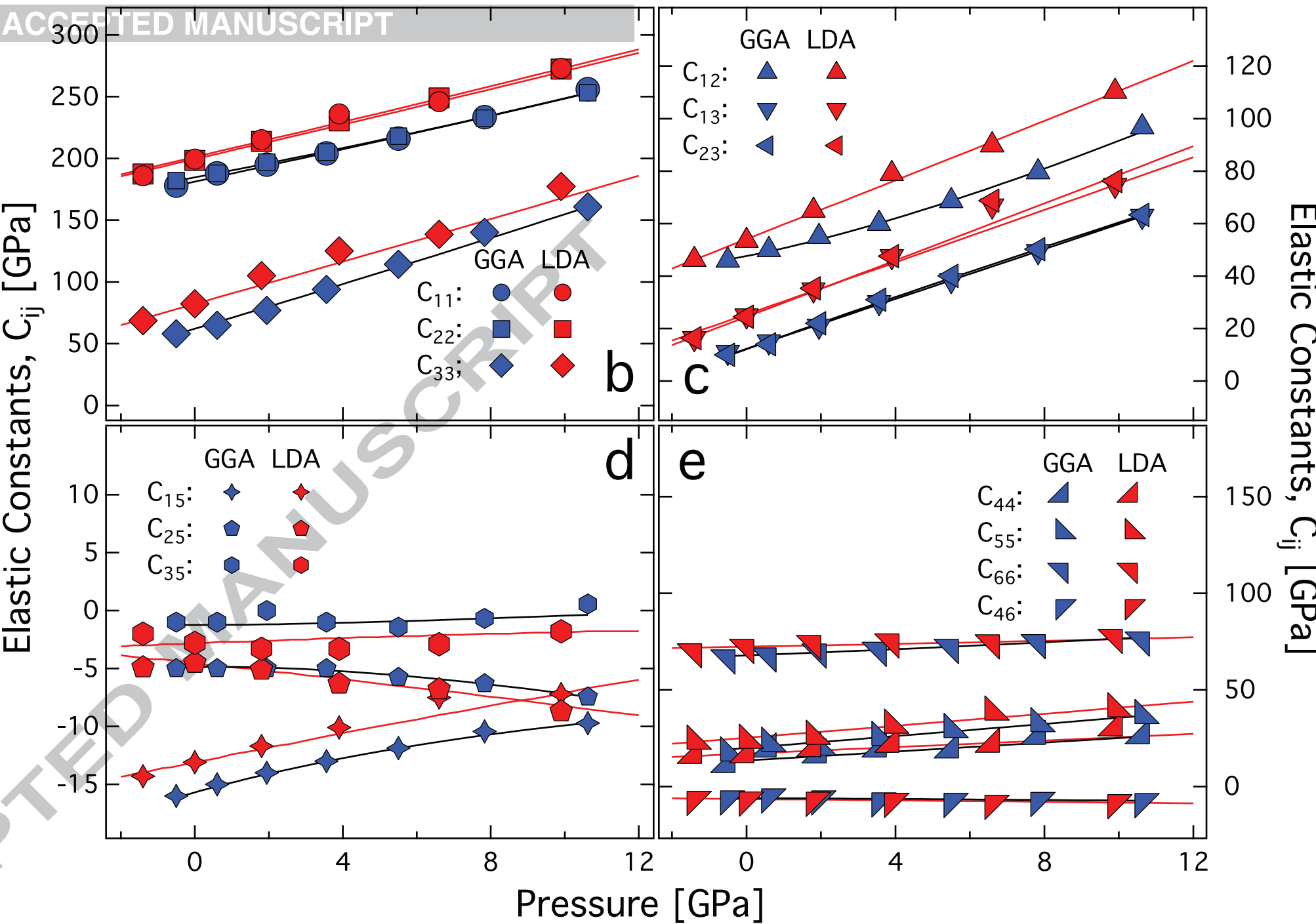
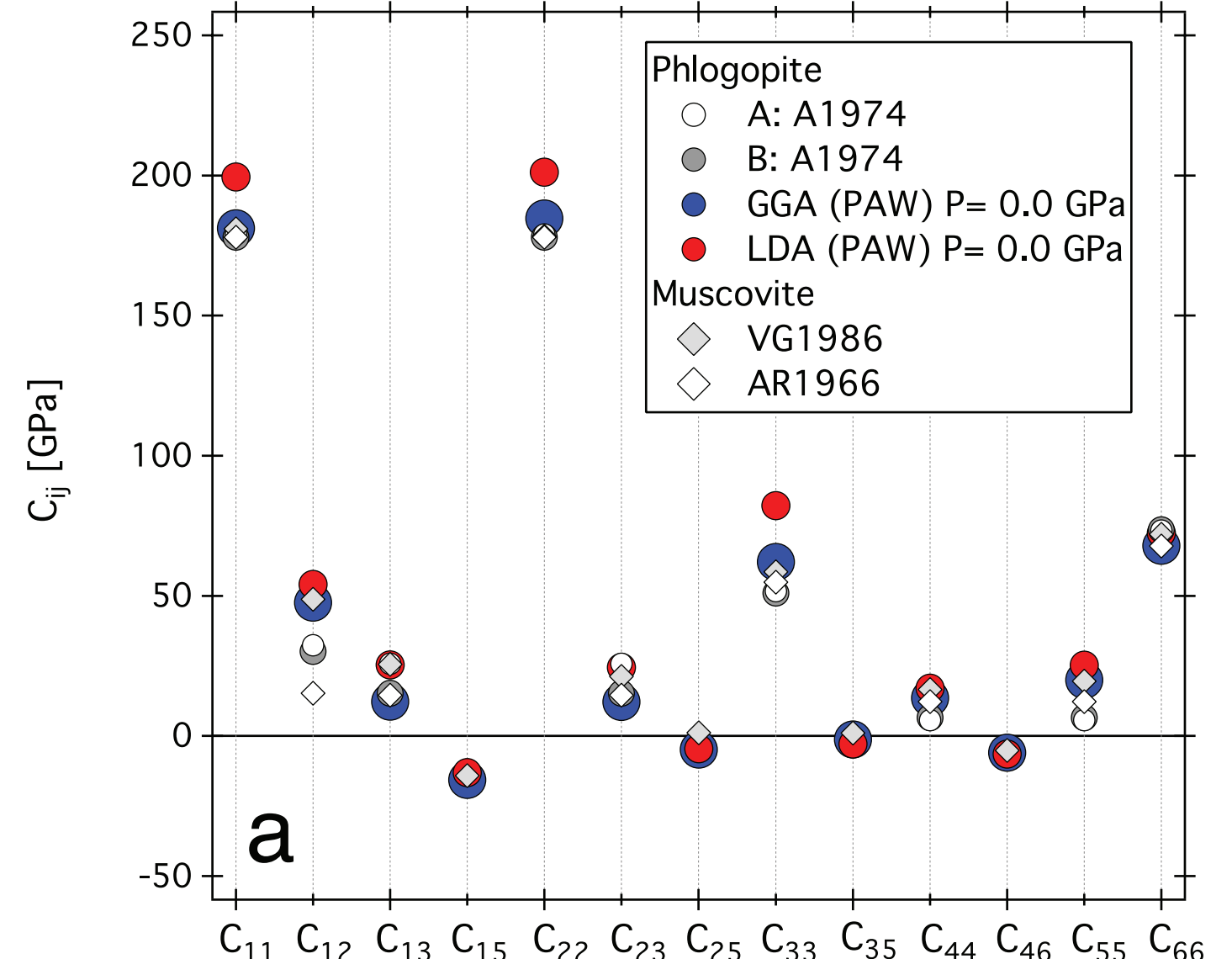
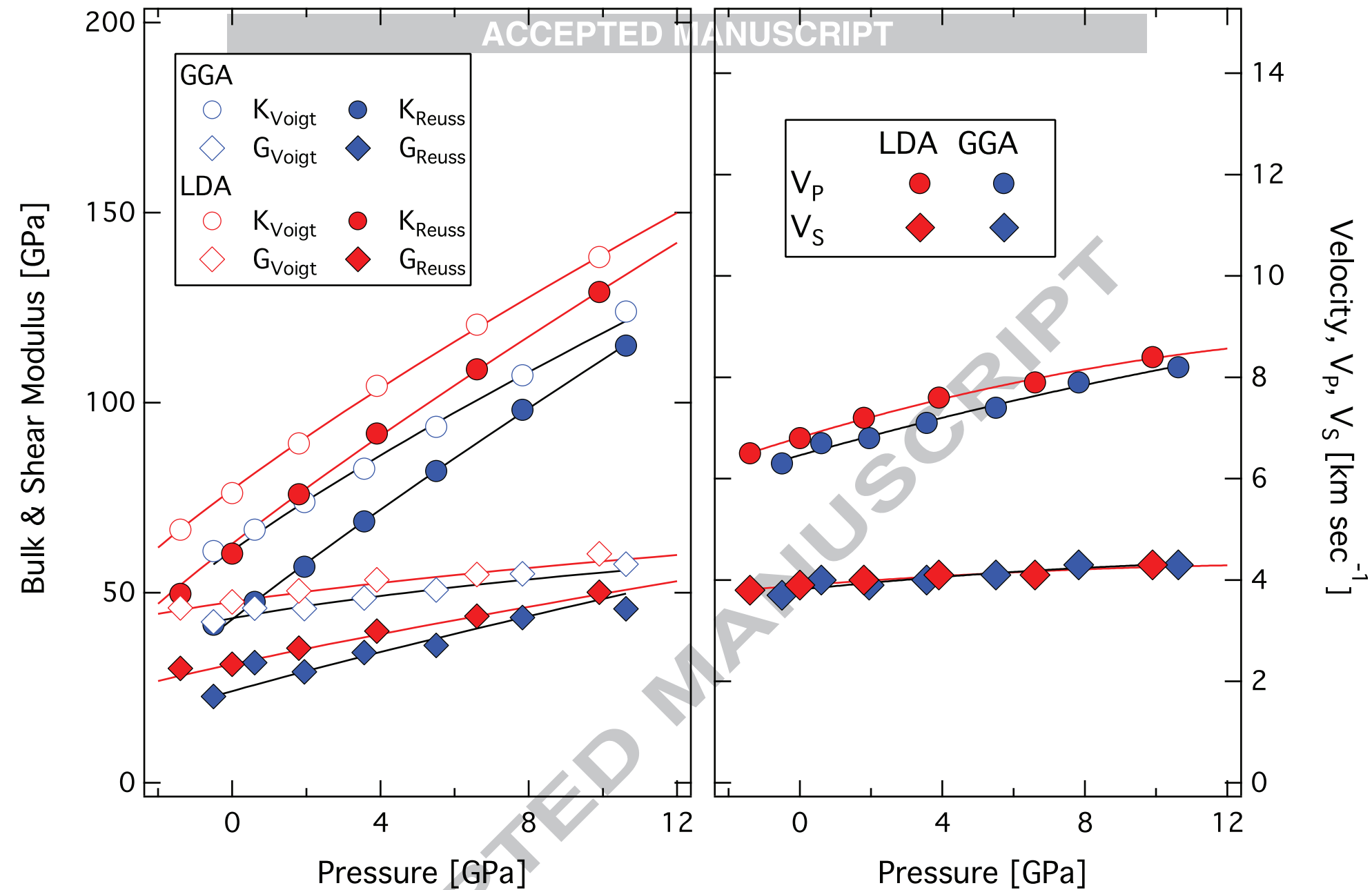


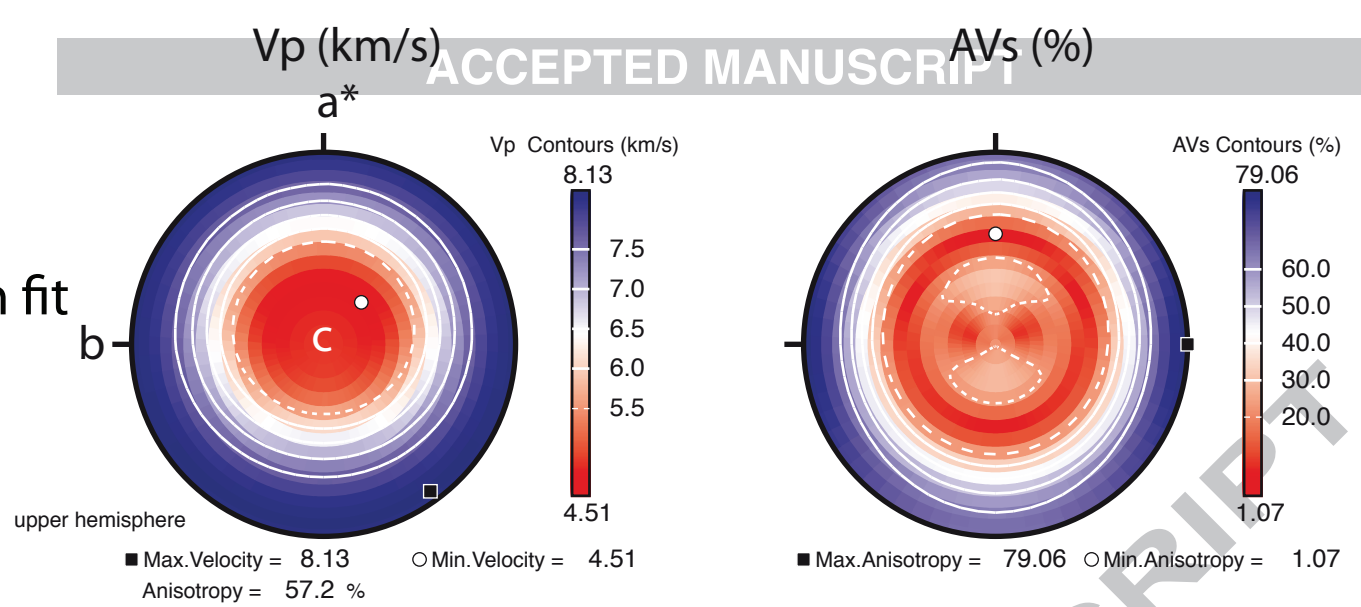
Figure 3



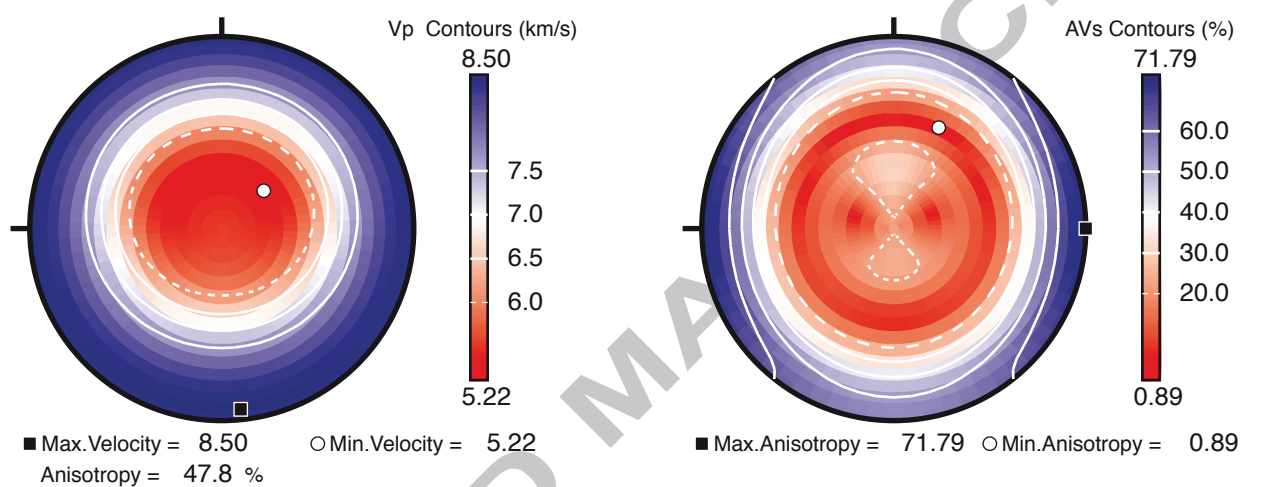




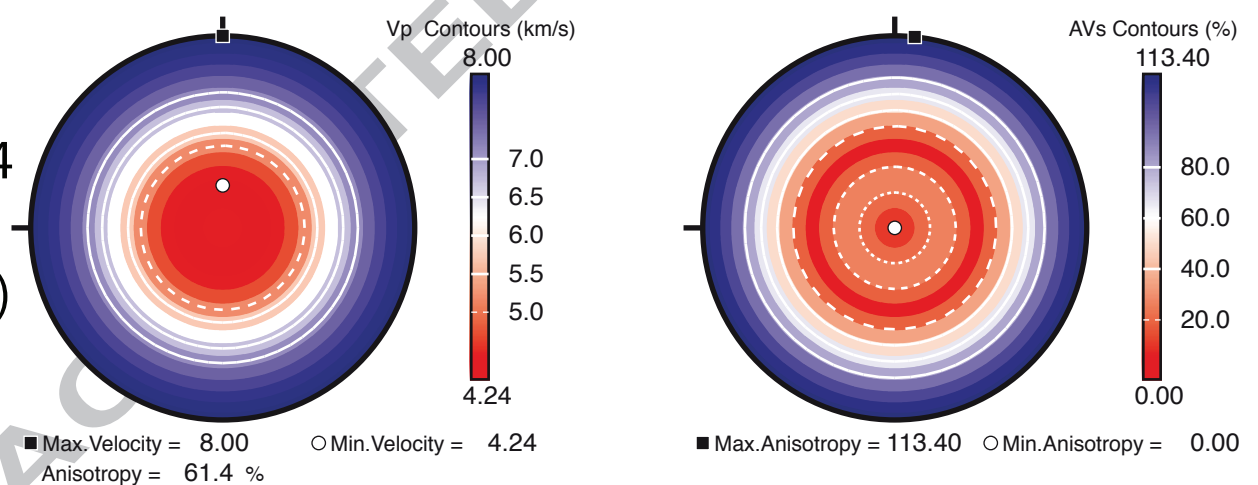
GGA Finite strain fit
P = 0 GPa



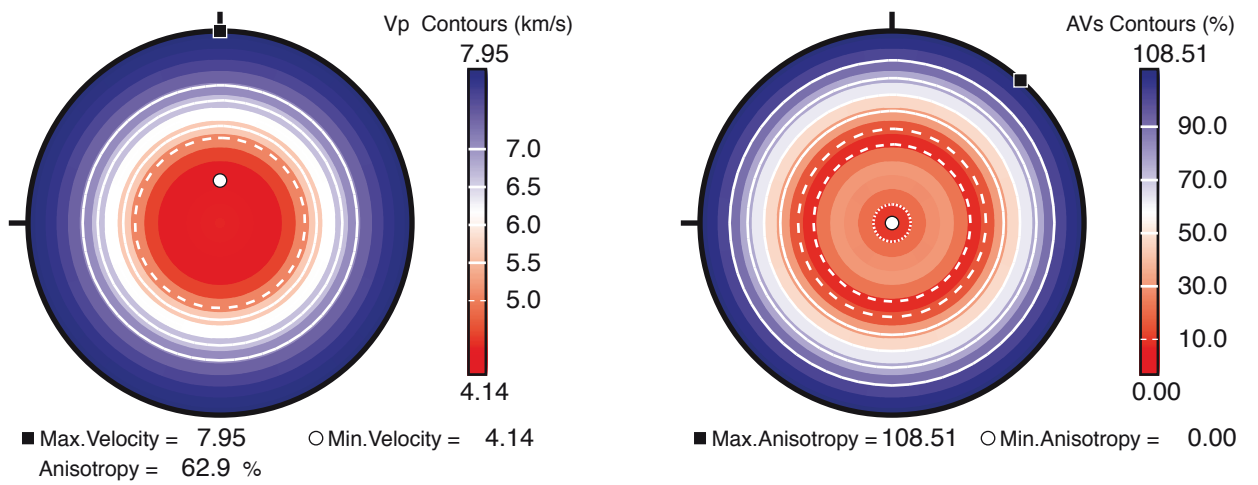
LDA Finite strain fit
P = 0 GPa

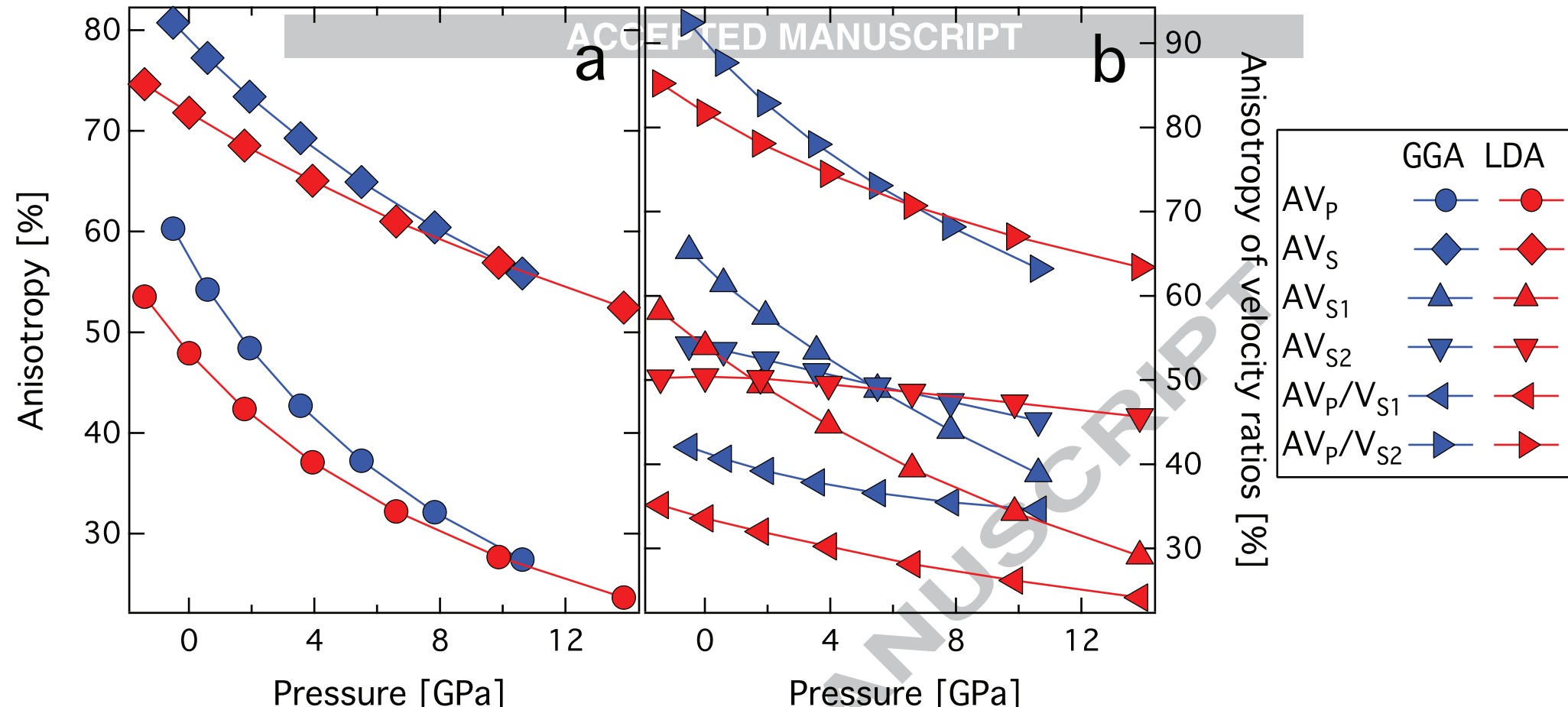


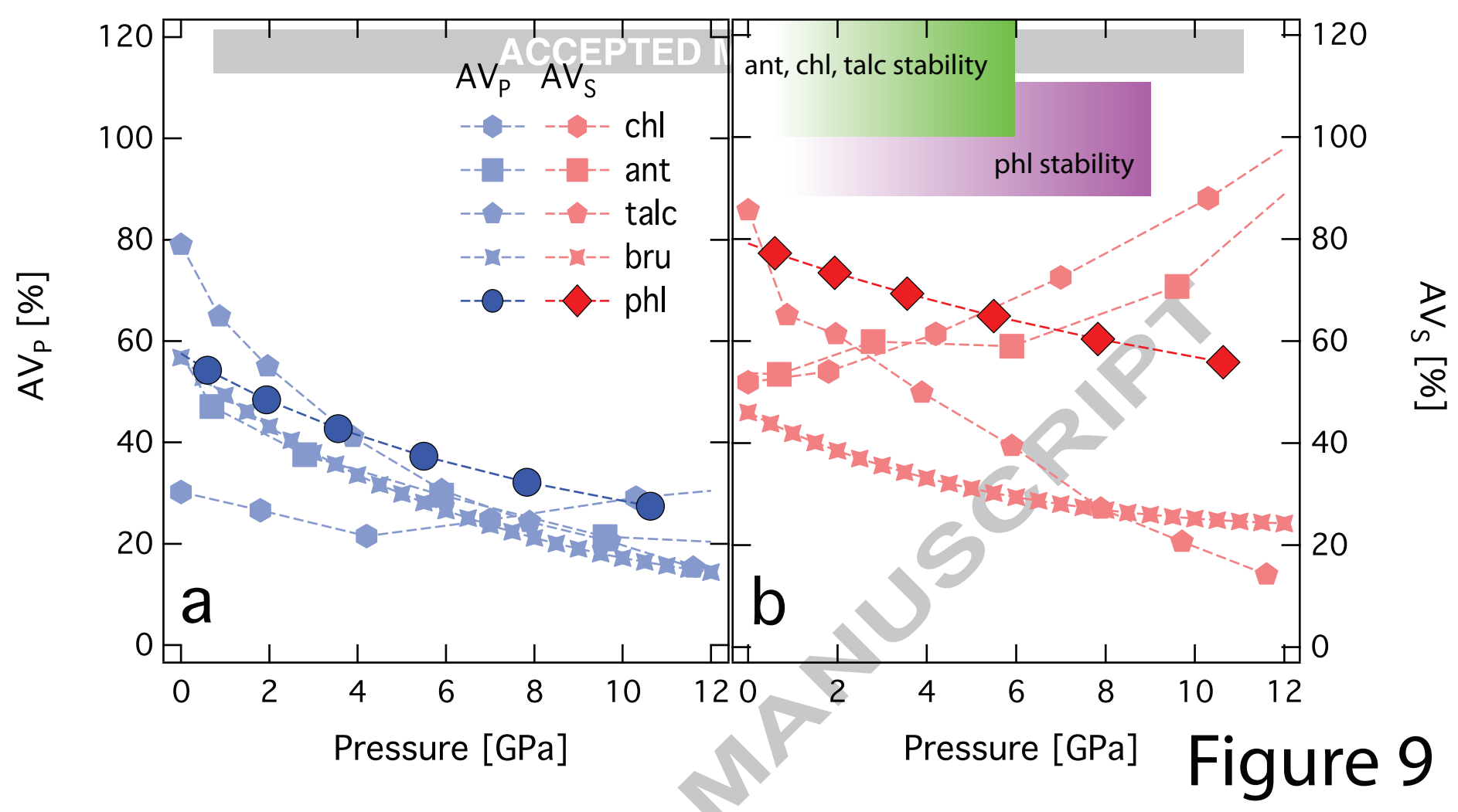
Alexandrov et al., 1974
Crystal A
(hexagonal symmetry)



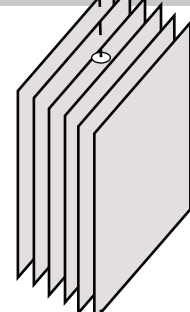
Alexandrov et al., 1974
Crystal B
(hexagonal symmetry)







seismic ray at
higher angles
w.r.t. (001) planes



seismic ray
(teleseismic)
near parallel to
(001) planes

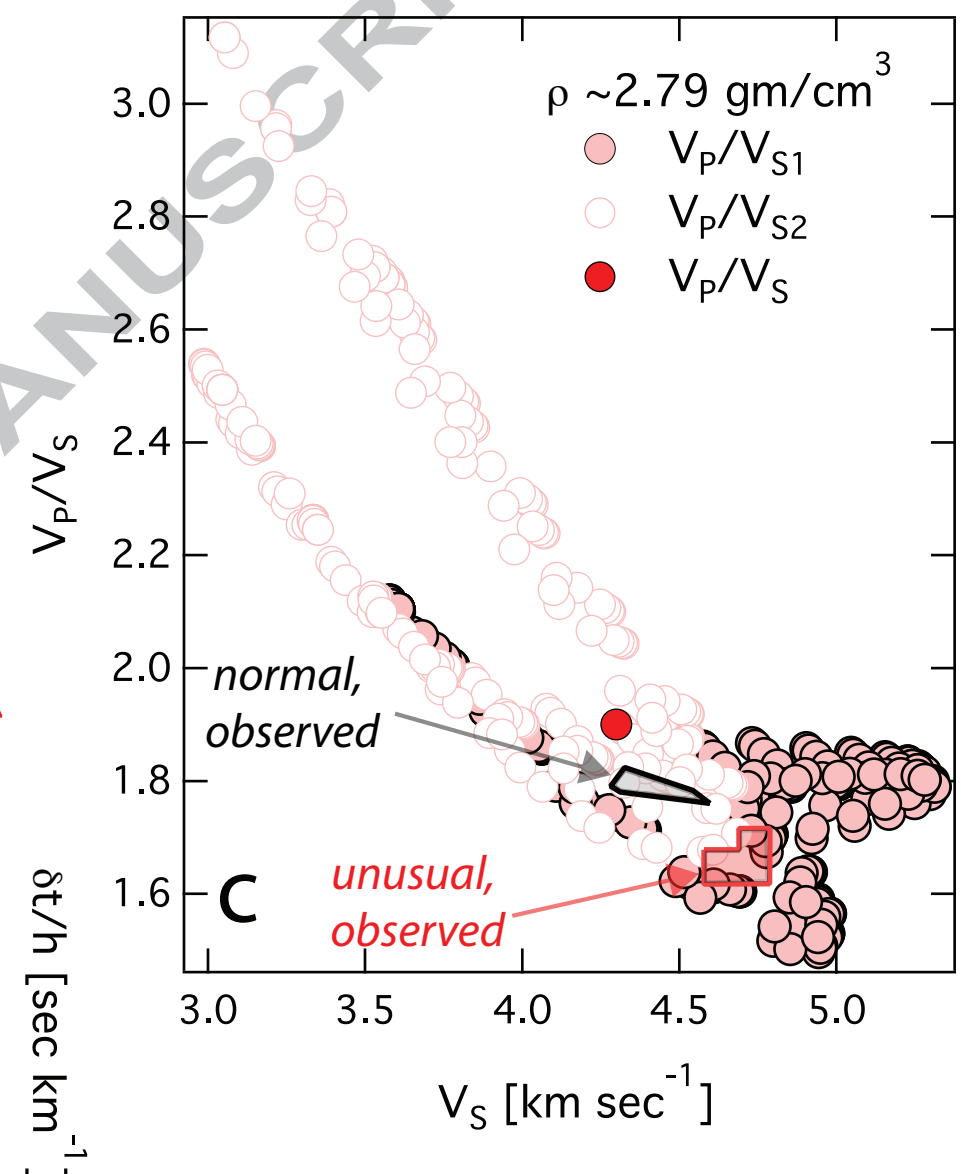
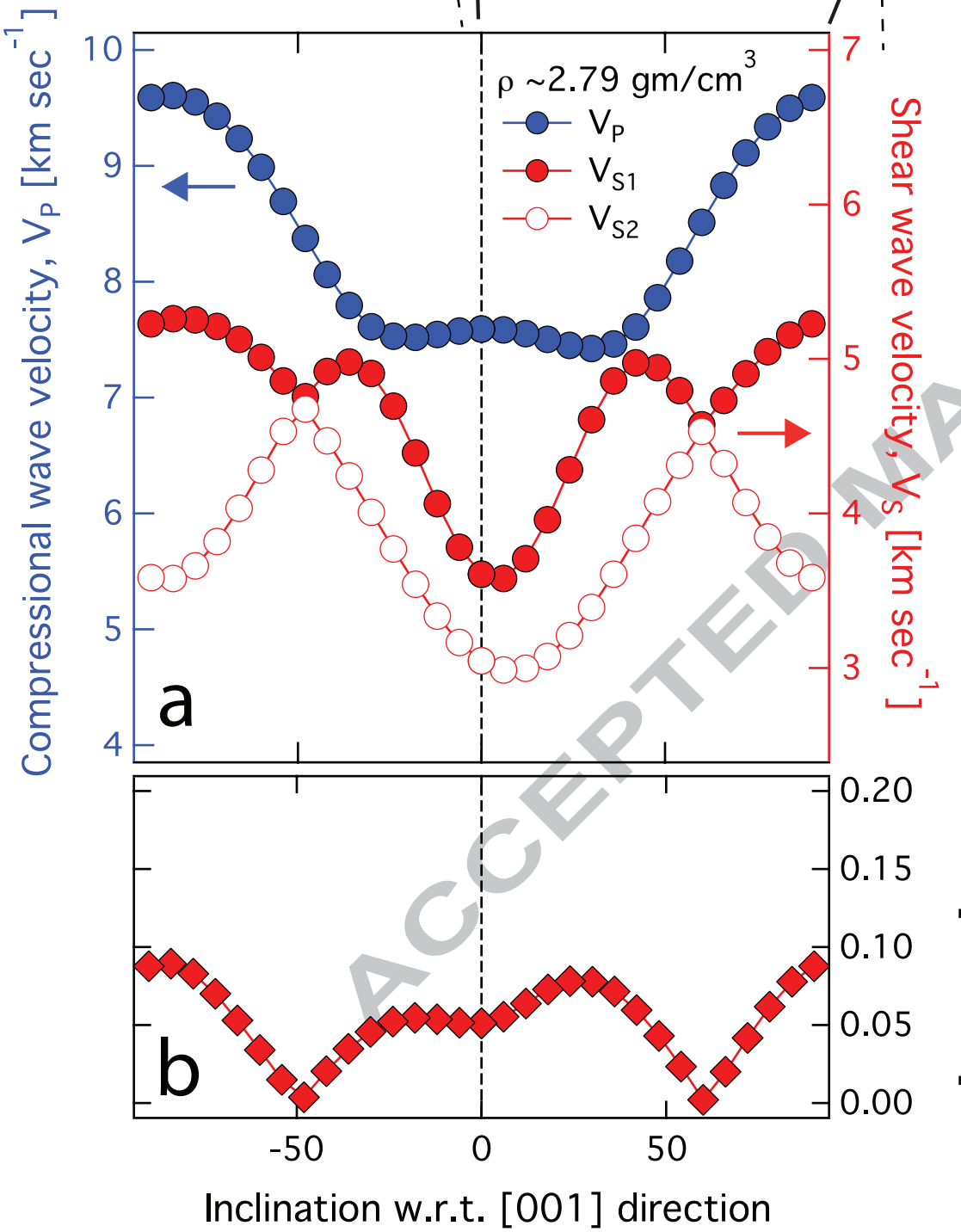


Figure 10

Table 1: Equation of state parameters for phlogopite.

E_0 [eV]	σ_{E0}	V_0 [\AA^3]	σ_{V0}	K_0 [GPa]	σ_{K0}	K'	$\sigma_{K'}$	Method
-652.44	0.05	473.03	1.06	60.8	4.3	8.1	1.7	LDA ¹
-595.30	0.04	518.72	1.08	41.6	2.5	10.1	1.3	GGA ¹
		488.64	0.20	49.7	0.5	8.6	0.2	SXRPD ²
		497.10	0.10	54.0	2.0	7.0	1.0	SCXRD ³
		487.70	0.20	58.5	2.0			SCXRD ⁴

1- this study;

LDA: Local Density Approximation

GGA: Generalized Gradient Approximation

2- Pavese et al. (2003); SXRPD: Synchrotron X-ray powder diffraction

3- Comodi et al. (2004); SCXRD: Single-Crystal X-ray diffraction

4- Hazen and Finger (1978); SCXRD: Single-Crystal X-ray diffraction

Table 2: Linear compressibility parameters for phlogopite.

a_0 [Å]	σ_{a0}	K_a [GPa]	σ_{Ka}	b_0 [Å]	σ_{b0}	K_b [GPa]	σ_{Kb}	c_0 [Å]	σ_{c0}	K_c [GPa]	σ_{Kc}	Method
5.238	0.007	395	21	9.086	0.007	406	20	10.200	0.007	84	25	LDA ¹
5.360	0.003	274	15	9.298	0.005	281	14	10.590	0.032	61	17	GGA ¹
5.314	0.001	287	4	9.199	0.002	313	10	10.153	0.003	76	1	SXRPD ²
5.336	0.001	123	9	9.240	0.003	128	15	10.237	0.006	25	2	SCXRD ³

1- this study;

LDA: Local Density Approximation

GGA: Generalized Gradient Approximation

2- Pavese et al. (2003); SXRPD: Synchrotron X-ray powder diffraction

3- Comodi et al. (2004); SCXRD: Single-Crystal X-ray diffraction

Table 3: Finite strain fit for the polyhedral units in phlogopite.

	$V_0 (\sigma_{V0})$ [Å ³]		$K_0 (\sigma_{KO})$ [GPa]	
KO ₁₂	72.9 (0.3)	64.6 (0.3)	21.1 (0.9)	28.7 (1.6)
MO ₆	12.14 (0.01)	11.35 (0.01)	112.1 (2.1)	152.7 (5.1)
TO ₄	2.43 (0.002)	2.30 (0.001)	241.7 (13.8)	287.0 (5.3)
Method	GGA	LDA	GGA	LDA

LDA: Local Density Approximation

GGA: Generalized Gradient Approximation

Table 4: Pressure dependence of the full elastic constant tensor (C_{ij}), bulk (K), and shear (G) modulus for phlogopite using *first principle* simulations. In addition, the finite strain fit results are also tabulated. The values in the bracket () denote the pressure derivatives.

V [Å ³]	P	C_{11}	C_{22}	C_{33}	C_{44}	C_{55}	C_{66}	C_{46}	C_{12}	C_{13}	C_{23}	C_{15}	C_{25}	C_{35}	K_V	K_R	G_V	G_R
[G Pa]																		
GGA(PAW)																		
525.0	-0.5	177.9	181.7	57.7	11.1	16.6	66.7	-5.9	45.5	10.6	9.6	-16.0	-4.6	-1.0	61.0	41.6	42.3	22.7
512.5	0.6	187.5	188.1	64.6	19.2	21.8	68.3	-5.4	50.4	15.0	14.1	-15.2	-4.9	-1.2	66.6	47.6	45.9	31.6
500.0	1.9	194.9	196.8	76.7	15.9	20.1	69.8	-6.2	55.2	20.9	21.9	-14.1	-4.7	-0.5	73.8	56.9	45.8	29.2
487.5	3.6	203.7	205.3	94.2	18.8	25.4	71.1	-6.6	59.7	29.6	30.9	-13.2	-5.2	-1.4	82.6	68.8	48.6	34.3
475.0	5.5	216.1	218.0	114.3	18.5	29.1	72.4	-7.2	68.7	38.4	40.1	-11.9	-5.8	-1.4	93.6	82.0	50.8	36.1
462.5	7.8	233.3	232.5	140.1	25.6	32.1	74.9	-6.8	79.7	49.4	50.3	-10.4	-6.3	-0.7	107.2	98.1	55.0	43.4
450.0	10.6	256.1	253.1	160.8	25.9	36.3	76.2	-7.3	96.8	62.8	63.3	-9.7	-7.5	0.6	124.0	115.0	57.5	45.7
finite strain fit																		
519.0	0	181.2	184.7	62.1	13.5	20.0	67.9	-5.9	47.6	12.2	12.1	-15.7	-4.9	-1.2	61.0	43.0	43.3	24.1
		(6.6)	(5.6)	(8.9)	(1.1)	(1.5)	(0.8)	(-0.1)	(2.8)	(4.8)	(5.1)	(0.9)	(0.04)	(-0.001)	(4.7)	(8.2)	(1.3)	(2.9)
LDA(PAW)																		
487.5	-1.4	185.9	187.3	68.6	15.8	23.1	70.2	-6.2	46.2	16.2	16.3	-14.3	-4.9	-2.0	66.6	49.7	46.0	30.1
475.0	0.0	199.5	198.4	82.2	16.1	23.5	72.4	-6.5	53.5	24.9	24.5	-13.1	-4.5	-2.8	76.2	60.3	47.6	31.2
462.5	1.8	215.2	213.7	105.1	19.2	25.6	74.5	-6.6	65.0	34.8	35.3	-11.7	-5.1	-3.3	89.3	75.9	50.5	35.4
450.0	3.9	236.1	230.3	125.1	21.5	31.4	75.2	-7.2	79.0	47.5	47.6	-10.1	-6.3	-3.3	104.4	91.9	53.4	39.9
437.5	6.6	245.9	249.0	138.5	21.5	38.2	74.8	-8.2	89.9	66.8	68.7	-7.5	-6.8	-2.9	120.5	108.8	54.8	43.8
425.0	9.9	272.8	272.3	177.3	30.0	39.8	77.6	-7.9	110.3	74.6	76.2	-7.2	-8.7	-1.8	138.3	129.1	60.2	50.1
412.5	13.9	291.6	294.1	199.9	28.9	47.0	76.4	-9.1	128.2	94.7	99.4	-5.4	-9.9	-1.7	158.9	150.5	61.4	51.1
finite strain fit																		
475.0	0	199.5	201.2	82.2	17.0	25.3	72.4	-6.4	54.1	25.4	24.4	-13.1	-4.5	-2.8	77.2	62.9	47.6	31.2
		(6.9)	(7.0)	(8.5)	(0.8)	(1.5)	(0.3)	(-0.2)	(5.6)	(5.0)	(5.4)	(0.6)	(-0.3)	(-0.001)	(5.6)	(7.2)	(1.1)	(2.0)

Highlights-

- (1) High-pressure elasticity of layered hydrous silicate- phlogopite
- (2) Unusually high shear wave anisotropy
- (3) Anisotropic V_P/V_S explains seismological observations

ACCEPTED MANUSCRIPT